Experimental study on the reaction rate of a second-order chemical reaction in a planar liquid jet

T. Watanabe,[1, a)] Y. Sakai,[1] K. Nagata,[1] and O. Terashima[1]

Department of Mechanical Science and Engineering, Nagoya University, Furo-cho, Chikusa-ku, Nagoya, Aichi, 464-8603, Japan

(Dated: 9 August 2022)

Instantaneous concentrations of reactive species are simultaneously measured in a planar liquid jet with a second-order chemical reaction A + B $\rightarrow$ R in order to investigate the statistical properties of the chemical reaction rate and the validity of models which have been proposed for concentration correlation. The jet flow contains the reactant A and the ambient flow contains the reactant B. The results show that the concentration correlation of the reactants makes a negative contribution to the mean reaction rate, and this contribution is important in the downstream direction. The concentration correlation changes owing to the chemical reaction. The effects of the chemical reaction on the concentration correlation change with the flow location and the Damköhler number. The concentration correlation predicted by the Toor's model and the three-environment (3E) model are compared with the experimental results. The results show that these models fail to accurately estimate the concentration correlation.

Keywords: Transport Phenomena, Diffusion (mass transfer, heat transfer), Fluid mechanics, Mixing, Turbulence

[a)]Research Fellow of the Japan Society for the Promotion of Science; watanabe.tomoaki@c.nagoya-u.jp

INTRODUCTION

Turbulent mixing with chemical reactions can take place in many pieces of industrial equipment and in the environment. Chemical reactions in combustors or chemical reactors and pollutant formation in the atmosphere are typical examples of chemical reactions in turbulent flows. Because turbulent flows have a great influence on chemical reactions and diffusion of reactive species, investigating the mechanism of interaction between turbulent flows and chemical reactions is important for predicting the efficiency of these types of equipment and the diffusion of pollutants.

The chemical reaction rate is one of the important quantities that characterize turbulent reactive flows. For a second-order chemical reaction $\mathrm{A} + \mathrm{B} \rightarrow \mathrm{R}$, the chemical reaction rate W, which represents the production rate of product species R, is given by

$$W = k\Gamma_{\mathrm{A}}\Gamma_{\mathrm{B}}, \tag{1}$$

where Γ_α is the instantaneous concentration of species α and k is the chemical reaction rate constant. Because of concentration fluctuations arising from turbulent motions, the instantaneous chemical reaction rate also spatiotemporally fluctuates and can be largely different from its mean value.

To numerically predict turbulent flows with scalar transfer, the Reynolds-averaged approach, in which averaged governing equations are numerically solved by using models, has been commonly used for various flows because of the low computational cost. The averaged transport equation for the concentration of reactive species α used in the Reynolds-averaged approach for turbulent reactive flows is given by[1]

$$\frac{\partial\langle\Gamma_\alpha\rangle}{\partial t} + \frac{\partial}{\partial x_j}(\langle U_j\rangle\langle\Gamma_\alpha\rangle) = \frac{\partial}{\partial x_j}(D_\alpha\frac{\partial}{\partial x_j}\langle\Gamma_\alpha\rangle) - \frac{\partial}{\partial x_j}\langle u_j\gamma_\alpha\rangle + \langle W_\alpha\rangle, \tag{2}$$

where U_i is the instantaneous i-direction velocity, D_α is the molecular diffusivity of species α, W_α is the production rate of species α by chemical reactions, and $\langle\ \rangle$ denotes an ensemble average. $u_i \equiv U_i - \langle U_i\rangle$ and $\gamma_\alpha \equiv \Gamma_\alpha - \langle\Gamma_\alpha\rangle$ are the fluctuating components of U_i and Γ_α, respectively. Models for the turbulent mass flux $\langle u_j\gamma_\alpha\rangle$ and the mean chemical reaction rate $\langle W_\alpha\rangle$ are required to solve Eq. (2). The gradient diffusion model[2] is widely used to predict the turbulent mass flux in numerical simulations of nonreactive flows. Although chemical reactions can affect the gradient diffusion hypothesis,[3–6] the gradient diffusion model is still

used to predict the turbulent mass flux of reactive species.[7,8] For the second-order chemical reaction $\mathrm{A} + \mathrm{B} \rightarrow \mathrm{R}$, the mean chemical reaction rate can be split into the product of mean concentrations of reactants A and B and the correlation of fluctuating concentrations of reactants A and B (hereafter, simply denoted as 'concentration correlation'):

$$\langle W \rangle = k\langle \Gamma_{\mathrm{A}} \rangle \langle \Gamma_{\mathrm{B}} \rangle + k\langle \gamma_{\mathrm{A}} \gamma_{\mathrm{B}} \rangle. \tag{3}$$

When the Reynolds-averaged approach is applied to turbulent flows with a second-order chemical reaction, the mean reaction rate is closed by using models for the concentration correlation term. The concentration correlation, $\langle \gamma_{\mathrm{A}} \gamma_{\mathrm{B}} \rangle$, is very sensitive to the flow geometry and type of chemical reactions. Therefore, $\langle \gamma_{\mathrm{A}} \gamma_{\mathrm{B}} \rangle$ in various flow fields and chemical reactions should be investigated to develop and verify the models for the concentration correlation term.

Measurements of the reaction rate of second-order chemical reactions require simultaneous measurements of the instantaneous concentrations of two reactants. Measurements of the reaction rate of second-order chemical reactions in a gaseous flow were conducted in a scalar mixing layer[3] and in a plume in grid turbulence.[9] Direct numerical simulation (DNS) was also used to investigate chemical reactions in turbulent flows at a low Schmidt number ($Sc = \nu/D \sim 1$, where ν is the kinematic viscosity).[10,11] The Batchelor scale, which is the smallest scale of concentration fluctuation, becomes small, being proportional to $Sc^{-1/2}$. Therefore, DNS of reactive flows is limited to flows at low Schmidt number, and investigations of chemical reactions in liquid flows, in which the Schmidt number is often much larger than 1, have been conducted through experiments. Concentration measurements in turbulent reactive flows are difficult to perform, especially in liquid flows. A few measurements of the reaction rate of second-order chemical reactions have been made in a scalar mixing layer[12] and in a confined jet.[13,14] Therefore, information on the chemical reaction rate in liquid flows is limited to these experimental results. Most of these previous experimental studies[12–14] on the reactive liquid flows have been conducted for a fast chemical reaction. Because the characteristics of chemical reactions in turbulent flows strongly depend on the reaction rate, experimental studies for reactive flows should be carried out for chemical reactions with various reaction rate constants.

The purpose of this study is to investigate the validity of the models which have been proposed for the concentration correlation by measuring instantaneous concentrations of

reactive species in a liquid jet with a second-order chemical reaction with a moderate reaction rate. We also investigate the statistical properties of the chemical reaction rate, which are important for modeling the concentration correlation. As mentioned above, measuring concentration of reactive species is a challenging problem especially in liquid flows. However, we have developed the measurement method for concentrations of multiple species in liquid flows in the previous studies.[15–21] A flow configuration is one of the important factors which determine mixing of chemical species. A planar jet investigated in this study is a typical example of free shear flows, and the fundamental characteristics of the flow fields are well investigated by numerical simulations[22–24] and experiments[25–27]. However, there is little information on chemical reactions in a planar liquid jet. In this study, the instantaneous concentrations of all reactive species are simultaneously measured in a planar liquid jet with a second-order chemical reaction, and we provide reliable data on the chemical reaction rate in the liquid jet. The validation of models for the concentration correlation is done by confirming whether the measured statistics satisfy the relationship which is assumed in the models. Furthermore, the mean concentration profile is numerically predicted using the models for the concentration correlation. The measurement results of the mean concentrations are compared with the prediction by the numerical simulation for investigating the validity of the models for the concentration correlation. First, the planar liquid jet with a second-order chemical reaction and the concentration measurement method are described in detail, and then the measurement results are given in this paper. Finally, conclusions are summarized in the last of the paper.

PLANAR LIQUID JET WITH A CHEMICAL REACTION

Figure 1 shows a snapshot of a planar liquid jet with a second-order chemical reaction $A + B \rightarrow R$. Here, the reactant A is 1-naphthol and the reactant B is diazotized sulfanilic acid. The product R is 4-(4′-sulphophenylazo)-1-naphthol, briefly referred to as monoazo dyestuff. The chemical reaction rate constant of this reaction is $k = 12000$ m^3/(mol·s).[28] The solution containing the reactant A is injected into the ambient flow containing the reactant B through a rectangular slit with a width of $d = 2$ mm. Additionally, nonreactive species C (Acid Blue 9, blue dyestuff), whose concentration can be considered as a conserved scalar, is added into the jet flow. The pH is kept constant by adding buffer salts (sodium

carbonate and sodium hydrogen carbonate) into the jet flow. The initial concentrations of the reactants A and B and the nonreactive species C are $\Gamma_{\mathrm{A0}} = 0.4$ mol/m^3, $\Gamma_{\mathrm{B0}} = 0.2$ mol/m^3, and $\Gamma_{\mathrm{C0}} = 0.1$ kg/m^3. The instantaneous concentration of the nonreactive species C, Γ_{C}, is used to define the mixture fraction:

$$\xi \equiv \frac{\Gamma_{\mathrm{C}}}{\Gamma_{\mathrm{C0}}}. \tag{4}$$

The jet flow and the ambient flow are supplied through the head tanks to keep the flow rates constant. The mean velocity at the jet exit is $U_{\mathrm{J}} = 1.29$ m/s, and the mean velocity of the ambient flow is $U_{\mathrm{M}} = 0.061$ m/s. The Reynolds number defined by $Re = (U_{\mathrm{J}} - U_{\mathrm{M}})d/\nu$ is 2200. The Schmidt number based on the molecular diffusivity of the nonreactive species C is $Sc \approx 600$. The Damköhler number is $Da = k(\Gamma_{\mathrm{A0}} + \Gamma_{\mathrm{B0}})d/(U_{\mathrm{J}} - U_{\mathrm{M}}) = 11.7$. As shown in Fig. 1, the origin of coordinate system is located at the center of the jet exit, and streamwise and cross-streamwise directions are represented by x and y, respectively.

CONCENTRATION MEASUREMENT METHOD

Instantaneous concentrations of dyestuffs (the product R and the nonreactive species C) are simultaneously measured by using the concentration measurement system based on light absorption spectrometry.[6,15–21] This system was recently improved in terms of the spatial resolution, and the improved system is shown in Fig. 2.[20,21] Two light-emitting diodes (LEDs), which have maximum light intensity at wavelengths of $\lambda_1 = 525$ nm (green) and $\lambda_2 = 625$ nm (red), respectively, are used as light sources. The light emitted by the two LEDs is fed to the sampling volume of an optical fiber probe through an optical fiber. The light passes through the sampling volume and is then split into two wavelengths ($\lambda_1 = 525$ nm and $\lambda_2 = 625$ nm) by the grating spectroscope. The light intensities of the split light are measured by a photomultiplier. The diameter of the optical fiber bundle used in the concentration measurement system is 0.1 mm, and the length of the sampling volume of the optical fiber probe is 0.5 mm.

When dyestuff species α is contained in the solution at the sampling volume, the light passing through the sampling volume is absorbed by the dyestuff solution. The intensity of incident light, I_0, and the intensity of transmitted light, I, are related to the instantaneous

concentration of species α as follows:

$$-\ln\frac{I(\lambda)}{I_0(\lambda)} = k_\alpha(\lambda)\Gamma_\alpha. \tag{5}$$

Here, $k_\alpha(\lambda)$ is a function of λ, which depends on the light absorption characteristics of species α and the length of the light path. When the solution contains multiple dyestuffs, $P(\lambda) \equiv -\ln(I(\lambda)/I_0(\lambda))$ is equal to the sum of each $P(\lambda)$ for the solution of single dyestuff. Therefore, $P(\lambda_n)$ for a solution of the dyestuffs R and C can be written as

$$P(\lambda_n) \equiv -\ln\frac{I(\lambda_n)}{I_0(\lambda_n)} = k_{\mathrm{R}}(\lambda_n)\Gamma_{\mathrm{R}} + k_{\mathrm{C}}(\lambda_n)\Gamma_{\mathrm{C}}. \tag{6}$$

$k_{\mathrm{R}}(\lambda_1)$, $k_{\mathrm{R}}(\lambda_2)$, $k_{\mathrm{C}}(\lambda_1)$, and $k_{\mathrm{C}}(\lambda_2)$ are determined by prior calibration experiments. $P(\lambda_1)$ and $P(\lambda_2)$ are measured by using the concentration measurement system. The instantaneous concentrations of R and C can then be determined from Eq. (6) for λ_1 and λ_2.

By using the mass conservation law,[3] the instantaneous concentrations of the reactants A and B can be determined from Γ_{R} and ξ:

$$\Gamma_{\mathrm{A}} = \xi\Gamma_{\mathrm{A0}} - \Gamma_{\mathrm{R}}, \tag{7}$$

$$\Gamma_{\mathrm{B}} = (1-\xi)\Gamma_{\mathrm{B0}} - \Gamma_{\mathrm{R}}. \tag{8}$$

Bilger et al.[3] defined the frozen limit as the limiting case of $k \to 0$ (the chemical reaction does not occur) and the equilibrium limit as the limiting case of $k \to \infty$ (the chemical reaction is infinitely fast). The instantaneous concentrations for the frozen limit, Γ_α^0, are given by

$$\Gamma_{\mathrm{A}}^0 \equiv \lim_{k\to 0}\Gamma_{\mathrm{A}} = \xi\Gamma_{\mathrm{A0}}, \tag{9}$$

$$\Gamma_{\mathrm{B}}^0 \equiv \lim_{k\to 0}\Gamma_{\mathrm{B}} = (1-\xi)\Gamma_{\mathrm{B0}}, \tag{10}$$

$$\Gamma_{\mathrm{R}}^0 \equiv \lim_{k\to 0}\Gamma_{\mathrm{R}} = 0. \tag{11}$$

The instantaneous concentrations for the equilibrium limit, Γ_α^∞, are given by

$$\Gamma_{\mathrm{A}}^\infty \equiv \lim_{k\to\infty}\Gamma_{\mathrm{A}} = (\Gamma_{\mathrm{A0}} + \Gamma_{\mathrm{B0}})(\xi - \xi_S)H(\xi - \xi_S), \tag{12}$$

$$\Gamma_{\mathrm{B}}^\infty \equiv \lim_{k\to\infty}\Gamma_{\mathrm{B}} = (\Gamma_{\mathrm{A0}} + \Gamma_{\mathrm{B0}})(\xi_S - \xi)H(\xi_S - \xi), \tag{13}$$

$$\Gamma_{\mathrm{R}}^\infty \equiv \lim_{k\to\infty}\Gamma_{\mathrm{R}} = \begin{cases} \Gamma_{\mathrm{A0}}\xi & (\xi < \xi_S) \\ \Gamma_{\mathrm{B0}}(1-\xi) & (\xi \geq \xi_S) \end{cases}. \tag{14}$$

Here, $H(z)$ is the Heaviside step function and ξ_{S} is the stoichiometric value of the mixture fraction given by $\xi_{\mathrm{S}} = \Gamma_{\mathrm{B0}}/(\Gamma_{\mathrm{A0}}+\Gamma_{\mathrm{B0}}) = 0.333$. The maximum concentration of the product R, Γ_{R0}, is obtained by substituting $\xi = \xi_{\mathrm{S}}$ and $\Gamma_{\mathrm{A}} = \Gamma_{\mathrm{B}} = 0$ in Eq. (7) or (8) and is given by $\Gamma_{\mathrm{R0}} = \Gamma_{\mathrm{A0}}\Gamma_{\mathrm{B0}}/(\Gamma_{\mathrm{A0}} + \Gamma_{\mathrm{B0}}) = 0.133$ mol/m^3.

The Kolmogorov scale and the Taylor microscale are $\eta_{\mathrm{K}} = 0.427$ mm and $\lambda_x = 2.32$ mm at $x/d = 20$ on the jet centerline,[17] respectively. The Batchelor scale, which is the smallest scale of scalar fluctuation, is $\eta_{\mathrm{B}} = \eta_{\mathrm{K}}/Sc^{1/2} = 0.0174$ mm. The spatial resolution of the optical fiber probe is related to the sampling volume $V_{\mathrm{P}} = 3.9\times10^{-3}$ mm^3, where the shape of the sampling volume is assumed to be a circular cylinder. The length scale corresponding to V_{P} is $l_{\mathrm{P}} = V_{\mathrm{P}}^{1/3} = 0.15$ mm. Thus, the spatial resolution of the concentration measurements is smaller than the Kolmogorov scale but is larger than the Batchelor scale.

The small-scale Damköhler number is defined by $Da_{\mathrm{Kol}} \equiv \tau_\eta/\tau_{\mathrm{R}}$, where $\tau_\eta \equiv (\nu/\epsilon)^{1/2}$ (ϵ: dissipation rate of turbulent kinetic energy) and $\tau_{\mathrm{R}} \equiv k^{-1}\langle\Gamma_{\mathrm{A}}\Gamma_{\mathrm{B}}\rangle^{-1/2}$ are the Kolmogorov timescale and the reaction timescale, respectively.[29,30] The small-scale Damköhler number at $x/d = 10$ and 40 is $Da_{\mathrm{Kol}} = 0.45$ and 0.74 on the jet centerline. It should be noted that in the measurement region, τ_{R} is smallest at $x/d = 10$ and τ_η on the jet centerline is largest at $x/d = 40$. Thus, the reaction is slow compared with the Kolmogorov timescale. An infinitely fast and irreversible chemical reaction occurs at the interface between the two reactants soon after the mixing at the molecular level. In this case, the reactants cannot coexist and the reaction zone thickness is infinitely thin because the reaction proceeds only at the interface until concentration of the deficient reactant becomes zero. However, the slow reaction used in this study occurs not only at the interface, and slowly proceeds after the two reactants are mixed well. Therefore, the length scale of the reaction zone of the slow reaction is larger than the Batchelor scale. The characteristics scale of passive scalar mixing larger than the Batchelor scale is mainly determined by the turbulent fields rather than the molecular diffusion.[1] Because the spatial resolution is smaller than the Kolmogorov scale, the reaction rate of the slow reaction can be measured by using the concentration measurement system described above. In this study, the concentration correlation of the two reactants is investigated in detail. By comparing the cospectra of the concentrations of the two reactants with the power spectra of the streamwise velocity in the next section, it is confirmed that the spatial resolution of the concentration measurement is sufficiently small for measuring the concentration correlation. The sampling volume of the new concentration measurement

system used in this study is 35 times smaller than that of the previous measurement system used for concentration measurements in the reactive liquid jet.[16–19] We also calculated the statistics relating to the chemical reaction rate using the previous measurement system, and confirmed that the same conclusions are derived from both measurement results independently of the spatial resolution. Thus, although the resolution is larger than the Batchelor scale, the measurement results in this study is useful for investigating the characteristics of the chemical reaction rate in the reactive liquid jet. Some of the measurement results obtained by the previous concentration measurement system have been presented in previous papers.[6,17–19]

RESULTS AND DISCUSSION

Mean velocity and mean concentrations

The mean velocity and the mean concentrations are shown to investigate the fundamental nature of the reactive planar jet. The streamwise velocity is measured by the X-type hot-film probe (TSI, 1248A-10W). The length and the diameter of two sensing elements of the X-type hot-film probe are 0.4 mm and 50.8 μm, respectively. The distance between two sensing elements of the X-type hot-film probe is 0.4 mm. Figure 3(a) shows the streamwise variation of the mean streamwise velocity on the jet centerline. Here, $\langle * \rangle_{\mathrm{C}}$ denotes the mean value on the jet centerline. In the self-similar region, the mean streamwise velocity on the jet centerline changes according to

$$\frac{U_{\mathrm{J}}^2}{(\langle U \rangle_{\mathrm{C}} - U_M)^2} = A_{U1}(x/d) + A_{U0}. \tag{15}$$

This relationship can be observed in Fig. 3(a). By applying the least-square method, we can obtain the coefficients $A_{U1} = 0.148$ and $A_{U0} = -0.0339$. Figure 3(b) shows the cross-streamwise profiles of $(\langle U \rangle - U_{\mathrm{M}})$ at different streamwise locations. In Fig. 3(b), the mean streamwise velocity is normalized by its value on the jet centerline, and the cross-streamwise coordinate y is normalized by the jet half-width b_U based on $\langle U \rangle - U_{\mathrm{M}}$. The self-similar profiles can be observed in the mean streamwise velocity. In the previous experimental measurement of velocity in a planar jet[27], the self-similar profile of the mean streamwise velocity is found to be given by the Gaussian curve, $\exp[-\ln 2(y/b_U)^2]$. Figure 3(b) shows

that the cross-streamwise profile of the mean streamwise velocity is well approximated by $\exp[-\ln 2(y/b_U)^2]$ in the planar liquid jet.

Figure 4(a) shows the mean mixture fraction on the jet centerline. Similar to the mean streamwise velocity, the mean mixture fraction on the jet centerline decreases in proportion to $(x/d)^{-1/2}$. The line obtained by the least-square method is also shown in Fig. 4(a). The cross-streamwise profiles of $\langle\xi\rangle/\langle\xi\rangle_{\mathrm{C}}$ are shown in Fig. 4(b). In this figure, the cross-streamwise coordinate y is normalized by the jet half-width b_ξ based on $\langle\xi\rangle$, and the Gaussian curve, $\exp[-\ln 2(y/b_\xi)^2]$, is also shown. The self-similar profile can be observed for the mean mixture fraction measured in this study. It is also found that the cross-streamwise profiles of $\langle\xi\rangle/\langle\xi\rangle_{\mathrm{C}}$ is well approximated by the Gaussian curve except at the edge of the jet. The deviation from the Gaussian curve can be also observed in the previous experiments.[25,26]

Figure 5 shows the streamwise evolution of the jet half-widths b_U and b_ξ. In the self-similar region, the jet half-widths b_U and b_ξ change according to

$$b_U/d = B_{U1}(x/d) + B_{U0}, \tag{16}$$

$$b_\xi/d = B_{\xi 1}(x/d) + B_{\xi 0}. \tag{17}$$

The relationships of Eqs. (16) and (17) can be seen in the measurement results of b_U and b_ξ in Fig. 5. Applying the least-square method to the measured b_U and b_ξ yields the coefficients $B_{U1} = 0.0738$, $B_{U0} = 0.0389$, $B_{\xi 1} = 0.125$, and $B_{\xi 0} = 0.133$. Thus, b_ξ is larger than b_U, and the spread rate based on the mean mixture fraction is larger than expected from the mean streamwise velocity. The similar tendency of b_U and b_ξ can be found in the planar jet investigated by the DNS[22] and the experiment.[25] Thus, the typical characteristics of self-similar region of a planar jet can be observed in the measurement results of the mean streamwise velocity and the mean mixture fraction.

The mean concentrations of the reactive species A, B, and R at $x/d = 10$, 20, and 40 are shown in Figs. 6, 7, and 8, respectively. In Fig. 8, $\langle\Gamma_{\mathrm{R}}\rangle$ measured in this study is compared with the previous measurement result obtained by the concentration measurement system whose sampling volume is 35 times larger than that of the present system. The mean concentrations of the reactants A and B for $Da = 11.7$ lie between those for the frozen and equilibrium limits. Figures 6(a) and 7(a) show that $\langle\Gamma_{\mathrm{A}}\rangle$ and $\langle\Gamma_{\mathrm{B}}\rangle$ for $Da = 11.7$ are close to the frozen limit at $x/d = 10$. At $x/d = 10$, the product concentration $\langle\Gamma_{\mathrm{R}}\rangle$ for $Da = 11.7$ (Fig. 8(a)) is much smaller than the equilibrium value. As x increases, the mean

concentration profiles approach the equilibrium limit. At $x/d = 40$ (Figs. 6(c), 7(c), and 8(c)), the mean concentration profiles are very close to the equilibrium limit. The mean concentration profile can be affected by the lack of spatial resolution. However, in Fig. 8, the large difference in $\langle \Gamma_{\mathrm{R}} \rangle$ between $Da = 11.8$ and the equilibrium limit is observed independently of the spatial resolution. This result shows that the chemical reaction used in the experiment is not fast. Because of the slow reaction, large amount of the reactant A which has not reacted exists at $x/d = 10$. As the reactant A is transported toward the downstream region, the mixing and the chemical reaction proceed. Therefore, the mean concentrations of reactive species approach the equilibrium limit in the downstream direction.

Mean reaction rate

The production rate of the normalized product concentration $\hat{\Gamma}_{\mathrm{R}} \equiv \Gamma_{\mathrm{R}}/\Gamma_{\mathrm{R0}}$ is given by $\hat{W} = Da\hat{\Gamma}_{\mathrm{A}}\hat{\Gamma}_{\mathrm{B}}$, where $\hat{\Gamma}_{\alpha} \equiv \Gamma_{\alpha}/\Gamma_{\alpha 0}$. According to Eq. (3), the normalized mean reaction rate $\langle \hat{W} \rangle$ can be written as

$$\langle \hat{W} \rangle = Da\langle \hat{\Gamma}_{\mathrm{A}} \rangle \langle \hat{\Gamma}_{\mathrm{B}} \rangle + Da\langle \hat{\gamma}_{\mathrm{A}} \hat{\gamma}_{\mathrm{B}} \rangle, \tag{18}$$

where the normalized concentration fluctuation is defined by $\hat{\gamma}_{\alpha} \equiv \gamma_{\alpha}/\Gamma_{\alpha 0}$.

Figure 9 shows the cross-streamwise profiles of $\langle \hat{W} \rangle$, $Da\langle \hat{\Gamma}_{\mathrm{A}} \rangle \langle \hat{\Gamma}_{\mathrm{B}} \rangle$, and $Da\langle \hat{\gamma}_{\mathrm{A}} \hat{\gamma}_{\mathrm{B}} \rangle$. $\langle \hat{W} \rangle$ decreases in the downstream direction. The small $Da\langle \hat{\Gamma}_{\mathrm{A}} \rangle \langle \hat{\Gamma}_{\mathrm{B}} \rangle$ in the downstream region suggests that the mean reaction rate decreases in the downstream direction because the chemical reaction reduces the concentrations of the reactants A and B. The fluctuating concentration correlation term $Da\langle \hat{\gamma}_{\mathrm{A}} \hat{\gamma}_{\mathrm{B}} \rangle$ makes a negative contribution to the mean reaction rate, and decreases in magnitude in the downstream direction. It is found that the chemical reaction mainly occurs near the jet centerline in the upstream region. The mean reaction rate weakly depends on the cross-streamwise position near the jet centerline. The cross-streamwise profiles of $Da\langle \hat{\gamma}_{\mathrm{A}} \hat{\gamma}_{\mathrm{B}} \rangle$ have two negative peak values at $|y/b_{\xi}| \approx 1$. At $x/d = 40$, $Da\langle \hat{\Gamma}_{\mathrm{A}} \rangle \langle \hat{\Gamma}_{\mathrm{B}} \rangle$ is small, especially in the outer region of the jet, because most of the reactant A is consumed by the chemical reaction before it can reach the downstream region. A comparison between $Da\langle \hat{\Gamma}_{\mathrm{A}} \rangle \langle \hat{\Gamma}_{\mathrm{B}} \rangle$ and $Da\langle \hat{\gamma}_{\mathrm{A}} \hat{\gamma}_{\mathrm{B}} \rangle$ shows that the contribution of the concentration correlation to the mean reaction rate becomes high in the downstream direction. Therefore, special attention should be paid to modeling the concentration correlation in the downstream region.

Probability density function of the reaction rate

Figure 10 shows the cross-streamwise variations of the probability density function (pdf) of the normalized reaction rate $\hat{W}$. From $y/b_\xi = 0$ toward $y/b_\xi = 1.5$ at $x/d = 10$, the contribution of the large reaction rate decreases and one of the small reaction rate increases, and the shape of the reaction rate pdf changes significantly in the cross-streamwise direction. However, from $y/b_\xi = 0$ toward $y/b_\xi = 1$ at $x/d = 20$, the reaction rate pdf is almost independent of the cross-streamwise location. At $y/b_\xi = 1.5$, the reaction rate pdfs at $x/d = 10$ and 20 have a large value at $\hat{W} \approx 0$ because the ambient fluid that is not mixed with the jet flow is detected in the outer region of the jet because of the outer intermittency.

The relationship between the concentrations of the reactants A and B is investigated by using the joint pdf of Γ_A and Γ_B. For the equilibrium limit, either of instantaneous concentrations of the reactants A or B is zero as shown in Eqs. (12) and (13), and the joint pdf of Γ_A and Γ_B has nonzero values only on the line of $\Gamma_\mathrm{A} = 0$ or $\Gamma_\mathrm{B} = 0$. Therefore, we calculate the joint pdf for the finite Damköhler number $Da = 11.7$. Figure 11 shows the joint pdf of Γ_A and Γ_B for $Da = 11.7$ at three different streamwise locations on the jet centerline. The white broken line in Fig. 11 shows $\Gamma_\mathrm{A}/\Gamma_{\mathrm{A}0} = 1 - \Gamma_\mathrm{B}/\Gamma_{\mathrm{B}0}$, which is satisfied by the concentrations for the frozen limit (Eqs. (9) and (10)). As shown in Fig. 11(a), the joint pdf of Γ_A and Γ_B at $x/d = 10$ maps near the line for the frozen limit. As x increases, the concentrations of the reactants A and B decrease because of the chemical consumption, and the joint pdf of Γ_A and Γ_B departs from the line of $\Gamma_\mathrm{A}/\Gamma_{\mathrm{A}0} = 1 - \Gamma_\mathrm{B}/\Gamma_{\mathrm{B}0}$. At $x/d = 10$ (Fig. 11(a)), the joint pdf maps for the region of $\Gamma_\mathrm{A}/\Gamma_{\mathrm{A}0} > \Gamma_\mathrm{B}/\Gamma_{\mathrm{B}0}$. Because the entrainment of the reactant B makes Γ_B large, the joint pdf at $x/d = 40$ (Fig. 11(c)) shows preference for $\Gamma_\mathrm{A}/\Gamma_{\mathrm{A}0} < \Gamma_\mathrm{B}/\Gamma_{\mathrm{B}0}$.

Concentration correlation of reactants

The following chemical reaction is considered to investigate the effect of the chemical reaction on the concentration correlation:

$$\mathrm{A} + n_\mathrm{B}\mathrm{B} \rightarrow n_\mathrm{R}\mathrm{R}. \tag{19}$$

The chemical reaction investigated in this study is obtained by substituting $n_\mathrm{B} = n_\mathrm{R} = 1$ into Eq. (19). For the chemical reaction given by Eq. (19), concentrations of the reactants

A and B are related to the mixture fraction and the concentration of the product R by using the mass conservation law as follows:

$$\Gamma_{\mathrm{A}} = \xi\Gamma_{\mathrm{A0}} - \frac{1}{n_{\mathrm{R}}}\Gamma_{\mathrm{R}}, \tag{20}$$

$$\Gamma_{\mathrm{B}} = (1-\xi)\Gamma_{\mathrm{B0}} - \frac{n_{\mathrm{B}}}{n_{\mathrm{R}}}\Gamma_{\mathrm{R}}. \tag{21}$$

The concentration fluctuations of the reactants A and B are then given by

$$\gamma_{\mathrm{A}} = \xi'\Gamma_{\mathrm{A0}} - \frac{1}{n_{\mathrm{R}}}\gamma_{\mathrm{R}}, \tag{22}$$

$$\gamma_{\mathrm{B}} = -\xi'\Gamma_{\mathrm{B0}} - \frac{n_{\mathrm{B}}}{n_{\mathrm{R}}}\gamma_{\mathrm{R}}. \tag{23}$$

Here, $\gamma_\alpha \equiv \Gamma_\alpha - \langle\Gamma_\alpha\rangle$ and $\xi' \equiv \xi - \langle\xi\rangle$. Using Eqs. (22) and (23), we can obtain the following expression for the concentration correlation of the reactants A and B:

$$\langle\gamma_{\mathrm{A}}\gamma_{\mathrm{B}}\rangle = \left\langle\left(\xi'\Gamma_{\mathrm{A0}} - \frac{1}{n_{\mathrm{R}}}\gamma_{\mathrm{R}}\right)\left(-\xi'\Gamma_{\mathrm{B0}} - \frac{n_{\mathrm{B}}}{n_{\mathrm{R}}}\gamma_{\mathrm{R}}\right)\right\rangle \tag{24}$$

$$= -\Gamma_{\mathrm{A0}}\Gamma_{\mathrm{B0}}\langle\xi'^2\rangle + \left(\frac{\Gamma_{\mathrm{B0}} - n_{\mathrm{B}}\Gamma_{\mathrm{A0}}}{n_{\mathrm{R}}}\right)\langle\xi'\gamma_{\mathrm{R}}\rangle + \frac{n_{\mathrm{B}}}{n_{\mathrm{R}}^2}\langle\gamma_{\mathrm{R}}^2\rangle. \tag{25}$$

When the chemical reaction does not occur, the concentration fluctuation of the product R, γ_{R}, is always equal to 0. Therefore, the concentration correlation in a nonreactive flow, $\langle\gamma_{\mathrm{A}}^0\gamma_{\mathrm{B}}^0\rangle$, is given by the first term in Eq. (25), i.e., $\langle\gamma_{\mathrm{A}}^0\gamma_{\mathrm{B}}^0\rangle = -\Gamma_{\mathrm{A0}}\Gamma_{\mathrm{B0}}\langle\xi'^2\rangle$. The second and third terms in Eq. (25) can be considered as the effects of the chemical reaction on the concentration correlation. For the chemical reaction given by Eq. (19), the stoichiometric ratio between the concentrations of the reactants A and B is $\Gamma_{\mathrm{A}}/\Gamma_{\mathrm{B}} = 1/n_{\mathrm{B}}$. When the initial concentrations of the reactants A and B satisfy the stoichiometric condition, the second term in Eq. (25) is always equal to 0. Therefore, the second term can be considered as the change in concentration correlation arising from the initial concentrations, which do not satisfy the stoichiometric condition.

The concentration correlation normalized by Γ_{A0} and Γ_{B0} can be written as

$$\langle\hat{\gamma}_{\mathrm{A}}\hat{\gamma}_{\mathrm{B}}\rangle = -\langle\xi'^2\rangle + (2\xi_{\mathrm{S}} - 1)\langle\xi'\hat{\gamma}_{\mathrm{R}}\rangle + \xi_{\mathrm{S}}(1-\xi_{\mathrm{S}})\langle\hat{\gamma}_{\mathrm{R}}^2\rangle, \tag{26}$$

where $\hat{\gamma}_\alpha \equiv \gamma_\alpha/\Gamma_{\alpha 0}$, ξ_{S} is the stoichiometric value of the mixture fraction, and Γ_{R0} is the maximum concentration of the product R. For the chemical reaction given by Eq. (19), ξ_{S}

and $\mathit{\Gamma}_{\mathrm{R0}}$ are defined by

$$\xi_{\mathrm{S}} = \frac{\mathit{\Gamma}_{\mathrm{B0}}}{n_{\mathrm{B}}\mathit{\Gamma}_{\mathrm{A0}} + \mathit{\Gamma}_{\mathrm{B0}}}, \tag{27}$$

$$\mathit{\Gamma}_{\mathrm{R0}} = \frac{n_{\mathrm{R}}\mathit{\Gamma}_{\mathrm{A0}}\mathit{\Gamma}_{\mathrm{B0}}}{n_{\mathrm{B}}\mathit{\Gamma}_{\mathrm{A0}} + \mathit{\Gamma}_{\mathrm{B0}}}. \tag{28}$$

Figure 12 shows the cross-streamwise profiles of $\langle\hat{\gamma}_{\mathrm{A}}\hat{\gamma}_{\mathrm{B}}\rangle$ for $Da = 11.7$ and each term in Eq. (26). Figure 13 shows the results for the equilibrium limit, where $\langle\hat{\gamma}_{\mathrm{A}}^{\infty}\hat{\gamma}_{\mathrm{B}}^{\infty}\rangle$ is the concentration correlation for the equilibrium limit and $\hat{\gamma}_{\alpha}^{\infty} \equiv \gamma_{\alpha}^{\infty}/\mathit{\Gamma}_{\alpha 0}$. To investigate the change in $\langle\hat{\gamma}_{\mathrm{A}}\hat{\gamma}_{\mathrm{B}}\rangle$ owing to the chemical reaction in detail, the cross-streamwise profiles of $\langle\hat{\gamma}_{\mathrm{A}}\hat{\gamma}_{\mathrm{B}}\rangle$ at $x/d = 10$ are also shown in Fig. 14, which is an enlargement of Fig. 12(a). In the region of $|y/b_{\xi}| > 1$ at $x/d = 10$, $\langle\hat{\gamma}_{\mathrm{A}}\hat{\gamma}_{\mathrm{B}}\rangle$ for $Da = 11.7$ (Figs. 12(a) and 14) becomes slightly larger in magnitude owing to the chemical reaction. However, except for this region, $\langle\hat{\gamma}_{\mathrm{A}}\hat{\gamma}_{\mathrm{B}}\rangle$ becomes small in magnitude owing to the chemical reaction. Comparing the results for $Da = 11.7$ (Fig. 12) with those for the equilibrium limit (Fig. 13), one sees that the fast chemical reaction (i.e., large Da) reduces the $\langle\hat{\gamma}_{\mathrm{A}}\hat{\gamma}_{\mathrm{B}}\rangle$ magnitude throughout the entire jet region. Thus, the effect of the chemical reaction on the concentration correlation depends on the Damköhler number. In the outer region of the jet at $x/d = 40$, $\hat{\gamma}_{\mathrm{A}}$ (Fig. 12(c)) and $\hat{\gamma}_{\mathrm{A}}^{\infty}$ (Fig. 13(c)) are always close to zero because the chemical reaction consumes most of the reactant A ejected from the jet exit before it can reach this region. Therefore, the concentration correlation for the reactive case is very small in the outer region of the jet at $x/d = 40$. It is also found that the cross-streamwise profiles of the concentration correlation have two negative peak values located away from the jet centerline.

The second term in Eq. (26), $(2\xi_{\mathrm{S}} - 1)\langle\xi'\hat{\gamma}_{\mathrm{R}}\rangle$, is positive near the jet centerline in the upstream region, but it is negative in the other regions. Thus, this term can be both positive and negative. However, because the third term in Eq. (26), $\xi_{\mathrm{S}}(1-\xi_{\mathrm{S}})\langle\hat{\gamma}_{\mathrm{R}}^2\rangle$, is always positive, $\xi_{\mathrm{S}}(1-\xi_{\mathrm{S}})\langle\hat{\gamma}_{\mathrm{R}}^2\rangle$ always contributes to the reduction of the concentration correlation magnitude. Comparison of $\xi_{\mathrm{S}}(1-\xi_{\mathrm{S}})\langle\hat{\gamma}_{\mathrm{R}}^2\rangle$ for $Da = 11.7$ with that for the equilibrium limit shows that the contribution of $\xi_{\mathrm{S}}(1-\xi_{\mathrm{S}})\langle\hat{\gamma}_{\mathrm{R}}^2\rangle$ to the concentration correlation becomes large as Da increases.

Because $(2\xi_{\mathrm{S}}-1) = -0.333 < 0$ in our experiment, the profiles of $(2\xi_{\mathrm{S}}-1)\langle\xi'\hat{\gamma}_{\mathrm{R}}\rangle$ explained above correspond to $\langle\xi'\hat{\gamma}_{\mathrm{R}}\rangle < 0$ near the jet centerline in the upstream region and $\langle\xi'\hat{\gamma}_{\mathrm{R}}\rangle > 0$ in the downstream and outer regions of the jet. Near the jet centerline in the upstream region, the deficient reactant is the reactant B contained in the ambient flow. Therefore, the high

chemical reaction rate is related to the positive concentration fluctuation of the deficient reactant B ($\hat{\gamma}_{\rm B} > 0$). When the chemical reaction rate is high, the concentration of the product R is supposed to be large ($\hat{\gamma}_{\rm R} > 0$). Because a positive concentration fluctuation of the reactant B corresponds to a negative mixture fraction fluctuation ($\xi' < 0$) as indicated in Eq. (23), $\langle \xi' \hat{\gamma}_{\rm R} \rangle$ is negative near the jet centerline in the upstream region. However, in the downstream and outer regions of the jet, the deficient reactant is the reactant A contained in the jet, resulting in $\langle \xi' \hat{\gamma}_{\rm R} \rangle > 0$. The sign of $(2\xi_{\rm S} - 1)$ depends on $\xi_{\rm S}$. Therefore, the effect of $(2\xi_{\rm S} - 1)\langle \xi' \hat{\gamma}_{\rm R} \rangle$ on the concentration correlation changes significantly with the location of the flow and the initial concentrations of reactants.

When the initial concentrations of the reactants A and B satisfy the stoichiometric condition, the concentration correlation for the reactive case is given by $\langle \hat{\gamma}_{\rm A} \hat{\gamma}_{\rm B} \rangle = -\langle \xi'^2 \rangle + \xi_{\rm S}(1 - \xi_{\rm S})\langle \hat{\gamma}_{\rm R}^2 \rangle$ because the second term in Eq. (26) is zero. In this case, the change of the concentration correlation caused by the chemical reaction is given by $\xi_{\rm S}(1-\xi_{\rm S})\langle \hat{\gamma}_{\rm R}^2 \rangle$. Because $\xi_{\rm S}(1 - \xi_{\rm S})\langle \hat{\gamma}_{\rm R}^2 \rangle \geq 0$ and $\xi_{\rm S}(1 - \xi_{\rm S})\langle \hat{\gamma}_{\rm R}^2 \rangle$ increases as Da becomes large (see Figs. 12 and 13), the concentration correlations for the frozen and equilibrium limits are the lower and higher bounds for the value for the finite Damköhler number:

$$\langle \gamma_{\rm A}^0 \gamma_{\rm B}^0 \rangle < \langle \gamma_{\rm A} \gamma_{\rm B} \rangle < \langle \gamma_{\rm A}^\infty \gamma_{\rm B}^\infty \rangle. \tag{29}$$

When Eq. (29) is valid, $\langle \gamma_{\rm A} \gamma_{\rm B} \rangle$ for the finite Damköhler number can be modeled by interpolating between the concentration correlations for the frozen limit and the equilibrium limit as suggested by by Bilger et al.[3] and de Bruyn Kops et al.[10] Figures 12(a) and 14 show that the concentration correlation for $Da = 11.7$ becomes large in magnitude owing to the chemical reaction in the region of $|y/b_\xi| > 1$ at $x/d = 10$. On the other hand, the concentration correlation for the equilibrium limit becomes small in magnitude owing to the chemical reaction throughout the entire jet region. Thus, the concentration correlations for the frozen and equilibrium limits are not the bounds for the value for the finite Damköhler number. This is because the initial concentrations of the reactants A and B do not satisfy the stoichiometric condition in our experiment. When the stoichiometric condition is not satisfied, the second term in Eq. (26) is not zero, and can make Eq. (29) invalid. Figure 15 shows the changes of $\xi_{\rm S}(1 - \xi_{\rm S})$ and $(2\xi_{\rm S} - 1)$, which are the coefficients of the second and the third terms in Eq. (26), with $\xi_{\rm S}$. It is found that, as $\xi_{\rm S}$ approaches 0 or 1, the change in the concentration correlation caused by the second term is expected to be much larger than

that caused by the third term. Therefore, Eq. (29) seems to be invalid under the condition of $\xi_S \approx 0$ or 1 because of the large contribution of the second term in Eq. (26).

Cospectra of concentrations of reactants

The cospectra of the concentrations of the reactants A and B, C_{AB}, are calculated for the finite Damköhler number $Da = 11.7$, the frozen limit, and the equilibrium limit. To investigate the relationship between the cospectra and the scales of the flow field, the power spectra of the streamwise velocity, E_u, are shown in Fig. 16. The power spectrum is multiplied by the frequency f. The peaks of fE_u at $x/d = 10$ and 40 appear at much smaller frequencies than the frequency corresponding to the dissipation scales. Thus, most of the energy of the velocity fluctuation is contained in much larger scales than the dissipation scales. Figure 17 shows the normalized cospectra $\hat{C}_{AB} \equiv C_{AB}/(\Gamma_{A0}\Gamma_{B0})$. The cospectrum is also multiplied by f to investigate the scales which largely contribute to the concentration correlation. It is found that $f\hat{C}_{AB}$ is large for the frequency range for which the power spectra fE_u in Fig. 16 are large. The results show that the large scales, which contain most of the energy of the velocity fluctuation, largely contribute to the concentration correlation in the planar jet. The concentration fluctuation on these large scales can be resolved well by the present concentration measurement system because the spatial resolution of the measurement system is smaller than the Kolmogorov scale. Therefore, the spatial resolution is sufficiently small for measuring the concentration correlation. Similar to $\langle\hat{\gamma}_A\hat{\gamma}_B\rangle$ in Fig. 12, the large difference in $f\hat{C}_{AB}$ can be observed between $Da = 11.7$ and the frozen limit at $x/d = 40$ as shown in Figs. 17(c) and (d). For the equilibrium limit, the change in $f\hat{C}_{AB}$ by the reaction is clearly found at both $x/d = 10$ and 40 in Fig. 17.

The infinitely fast and irreversible reaction is expected to occur in the interfacial region of the two reactants, whose thickness is infinitely thin. However, the cospectra for the equilibrium limit show that the concentration correlation is affected at large scales by the fast reaction. Figure 18 shows the instantaneous concentrations of the reactants A and B. At $(x, y) = (20d, 0)$, the reactant B is deficient, and Γ_B frequently becomes zero for the equilibrium limit. At $(x, y) = (20d, b_\xi)$, one of the reactants A and B is often completely consumed for the equilibrium limit. The concentration fluctuations at large scales are related to a lump of the reactants. When a fast reaction occurs, the lump of the reactants often

disappears because most of the reactants in the lump are reacted as confirmed in Γ_A and Γ_B for the equilibrium limit in Fig. 18. Therefore, the fast chemical reaction largely affects the concentration fluctuations at large scales although the fast reaction itself occurs at small scales. The reaction also affects the small scale concentration fluctuations, and the reaction effects begin with the small scales. These initial effects at the small scales are expected to be important in the initial shear layer of the planar jet, which appears very close to the jet exit. In this study, the measurements are conducted in the self-similar region. This is the reason that the cospectra greatly change at large scales for the equilibrium limit. Because the concentration fluctuations on the large scales largely contribute to the concentration correlation, the change in the large-scale fluctuations by the reaction makes the difference in the concentration correlation between the reactive and nonreactive cases.

As described above, the effects of the chemical reaction on the concentration correlation greatly change with the location and the Damköhler number. Therefore, predicting accurately the effect of the chemical reaction on the concentration correlation is very important for modeling the concentration correlation.

Models for concentration correlation

Various models for the concentration correlation, $\langle \gamma_A \gamma_B \rangle$, have been previously proposed for chemical reactions in a plug-flow reactor.[31–34] Because the flow and the chemical reaction in the ideal plug-flow reactor can be considered to be statistically one-dimensional, models for $\langle \gamma_A \gamma_B \rangle$ proposed for the plug-flow reactor cannot be applied for chemical reactions in multidimensional flows. In this section, the measured concentration correlation is compared with the models of Toor[32] and Dutta and Tarbell[34], which are extended to chemical reactions in multidimensional flows by Wang and Tarbell[7], and the validity of these models are discussed.

Toor developed the model for $\langle \gamma_A \gamma_B \rangle$ by assuming that the segregation intensity $I_S \equiv \langle \gamma_A \gamma_B \rangle / (\langle \Gamma_A \rangle \langle \Gamma_B \rangle)$ is independent of chemical reactions. This model is called "Toor's hypothesis." The segregation intensity in a nonreactive flow, I_S^0, can be written as

$$I_S^0 = \frac{\langle \gamma_A^0 \gamma_B^0 \rangle}{\langle \Gamma_A^0 \rangle \langle \Gamma_B^0 \rangle} = -\frac{\langle \xi'^2 \rangle}{\langle \xi \rangle (1 - \langle \xi \rangle)}. \tag{30}$$

By using Toor's hypothesis, the concentration correlation $\langle \hat{\gamma}_A \hat{\gamma}_B \rangle$ in multidimensional flows[7]

is modeled by

$$\langle \hat{\gamma}_{\mathrm{A}} \hat{\gamma}_{\mathrm{B}} \rangle = -\frac{\langle \xi'^2 \rangle}{\langle \xi \rangle (1 - \langle \xi \rangle)} \langle \mathit{\Gamma}_{\mathrm{A}} \rangle \langle \mathit{\Gamma}_{\mathrm{B}} \rangle / \mathit{\Gamma}_{\mathrm{A0}} \mathit{\Gamma}_{\mathrm{B0}}. \tag{31}$$

The segregation intensity is the measure of unmixedness of two reactants. When two reactants are unmixed, the two reactants are fully segregated. With the mixing of two reactants, the segregation intensity becomes small in magnitude. However, the chemical product is produced by the chemical reaction, which occurs after mixing of the two reactants. The presence of the chemical product makes the two reactants segregated. Thus, the segregation intensity is affected by the production of the chemical product. The change in the segregation intensity by chemical reactions has been observed in a reactive scalar mixing layer in liquid[12], where the heat release and the change in density by the chemical reaction can be neglected. Thus, it has been pointed out that Toor's hypothesis is not valid, and the segregation intensity decreases owing to the chemical reaction.[12] However, the Toor's model can still be useful if the change in segregation intensity caused by the chemical reaction is small.

Dutta and Tarbell[34] proposed the three-environment (3E) model, in which the concentration correlation in multidimensional flows[7] is given by

$$\langle \hat{\gamma}_{\mathrm{A}} \hat{\gamma}_{\mathrm{B}} \rangle = I_{\mathrm{S}}^0 \left(\langle \mathit{\Gamma}_{\mathrm{A}}^0 \rangle \langle \mathit{\Gamma}_{\mathrm{B}} \rangle + \langle \mathit{\Gamma}_{\mathrm{A}} \rangle \langle \mathit{\Gamma}_{\mathrm{B}}^0 \rangle - \langle \mathit{\Gamma}_{\mathrm{A}} \rangle \langle \mathit{\Gamma}_{\mathrm{B}} \rangle \right) / \mathit{\Gamma}_{\mathrm{A0}} \mathit{\Gamma}_{\mathrm{B0}} \tag{32}$$

$$= -\frac{\langle \xi'^2 \rangle}{\langle \xi \rangle (1 - \langle \xi \rangle)} \left(\langle \mathit{\Gamma}_{\mathrm{A}}^0 \rangle \langle \mathit{\Gamma}_{\mathrm{B}} \rangle + \langle \mathit{\Gamma}_{\mathrm{A}} \rangle \langle \mathit{\Gamma}_{\mathrm{B}}^0 \rangle - \langle \mathit{\Gamma}_{\mathrm{A}} \rangle \langle \mathit{\Gamma}_{\mathrm{B}} \rangle \right) / \mathit{\Gamma}_{\mathrm{A0}} \mathit{\Gamma}_{\mathrm{B0}}. \tag{33}$$

Here, $\langle \mathit{\Gamma}_{\mathrm{A}}^0 \rangle = \langle \xi \rangle \mathit{\Gamma}_{\mathrm{A0}}$ and $\langle \mathit{\Gamma}_{\mathrm{B}}^0 \rangle = (1 - \langle \xi \rangle) \mathit{\Gamma}_{\mathrm{B0}}$ can be obtained from Eqs. (9) and (10). To estimate $\langle \hat{\gamma}_{\mathrm{A}} \hat{\gamma}_{\mathrm{B}} \rangle$ by using Eqs. (31) and (33), $\langle \xi \rangle$ and $\langle \xi'^2 \rangle$ have to be calculated by other methods. In this paper, the concentration correlations for $Da = 11.7$ and the equilibrium limit are predicted by the Toor's model and the 3E model by using the measured values of $\langle \xi \rangle$ and $\langle \xi'^2 \rangle$, and the changes in the concentration correlation caused by the chemical reaction predicted by the Toor's model and the 3E model are compared with the experimental results. The models for the concentration correlation are validated by confirming whether the measured statistics satisfy Eqs. (31) and (33) or not.

The cross-streamwise profiles of $\langle \hat{\gamma}_{\mathrm{A}} \hat{\gamma}_{\mathrm{B}} \rangle$ and $\langle \hat{\gamma}_{\mathrm{A}}^{\infty} \hat{\gamma}_{\mathrm{B}}^{\infty} \rangle$ predicted by the Toor's model and the 3E model are compared with the experimental results in Figs. 19 and 20, respectively. In these figures, the cross-streamwise profiles of the concentration correlation in the nonreactive flow, $\langle \hat{\gamma}_{\mathrm{A}}^0 \hat{\gamma}_{\mathrm{B}}^0 \rangle$, are also shown, where $\hat{\gamma}_{\alpha}^0 \equiv \gamma_{\alpha}^0 / \mathit{\Gamma}_{\alpha 0}$. The concentration correlation predicted

by the Toor's model is small in magnitude compared with the experimental results. The 3E model well predicts $\langle\hat{\gamma}_A\hat{\gamma}_B\rangle$ at $x/d = 10$. However, throughout the entire jet region, $\langle\hat{\gamma}_A\hat{\gamma}_B\rangle$ predicted by the 3E model is small in magnitude compared with the concentration correlation in the nonreactive flow. In contrast, the measurement results of $\langle\hat{\gamma}_A\hat{\gamma}_B\rangle$ show that $\langle\hat{\gamma}_A\hat{\gamma}_B\rangle$ becomes large in magnitude owing to the chemical reaction in the region of $|y/b_\xi| > 1$ at $x/d = 10$. Thus, the effect of the reaction on $\langle\hat{\gamma}_A\hat{\gamma}_B\rangle$ predicted by the 3E model exhibits the opposite tendency from the experimental results. These results show that the 3E model is not adequate in the region of $|y/b_\xi| > 1$ at $x/d = 10$. It is also found that the 3E model well predicts the concentration correlation in the region where the change in the concentration correlation caused by the chemical reaction is small, whereas the error of the 3E model becomes large for the case in which the concentration correlation is largely affected by the chemical reaction.

Figures 19 and 20 suggest that the Toor's model and the 3E model are inadequate for modeling chemical reactions in a jet flow. Wang and Tarbell[7] pointed out that the Toor's model and the 3E model neglect the change in the mean concentration gradient caused by the chemical reaction, and they modified these models to take into account the change in the mean concentration gradient. They showed that this modification improved both the Toor's model and the 3E model. The modified models cannot be verified by using our experimental results. However, the poor predictions of concentration correlation from the Toor's model and the 3E model in this study are supposed to arise from neglecting the change in mean concentration gradient caused by the chemical reaction.

Numerical simulation of the reactive planar liquid jet based on the averaged transport equation

Governing equations of mean concentration fields and numerical method

To investigate the validity of the models for the concentration correlation, we perform the numerical simulation of the reactive planar jet investigated in this study. The mean concentration profiles are numerically predicted by using the averaged transport equation for the concentration (Eq. (2)). The concentration correlation term is modeled by the Toor's model or the 3E model. We compare the mean concentration profiles between the

experiment and the numerical simulation to investigate the influence of the concentration correlation models on the mean concentration prediction.

The self-similar region of the planar jet is simulated. The statistics in the planar jet are independent of the spanwise direction. The planar jet is statistically symmetrical with respect to the x-axis ($y = 0$). In the planar jet, the averaged transport equations for the mixture fraction and the concentration of the reactant A are given by

$$\langle U\rangle\frac{\partial\langle\xi\rangle}{\partial x} + \langle V\rangle\frac{\partial\langle\xi\rangle}{\partial y} = D\left(\frac{\partial^2\langle\xi\rangle}{\partial x^2} + \frac{\partial^2\langle\xi\rangle}{\partial y^2}\right) - \frac{\partial}{\partial x}\langle u\xi'\rangle - \frac{\partial}{\partial y}\langle v\xi'\rangle, \tag{34}$$

$$\begin{aligned}\langle U\rangle\frac{\partial\langle\Gamma_{\mathrm{A}}\rangle}{\partial x} + \langle V\rangle\frac{\partial\langle\Gamma_{\mathrm{A}}\rangle}{\partial y} = D\left(\frac{\partial^2\langle\Gamma_\alpha\rangle}{\partial x^2} + \frac{\partial^2\langle\Gamma_\alpha\rangle}{\partial y^2}\right) - \frac{\partial}{\partial x}\langle u\gamma_{\mathrm{A}}\rangle - \frac{\partial}{\partial y}\langle v\gamma_{\mathrm{A}}\rangle \\ - k\left(\langle\Gamma_{\mathrm{A}}\rangle\langle\Gamma_{\mathrm{B}}\rangle + \langle\gamma_{\mathrm{A}}\gamma_{\mathrm{B}}\rangle\right).\end{aligned} \tag{35}$$

Here, U is the streamwise velocity, V is the cross-streamwise velocity, and u and v are the fluctuating components of U and V, respectively. In Eqs. (34) and (35), the equal molecular diffusivity D is assumed for all reactive species and the mixture fraction. The mean concentrations of the reactant B and the product R can be obtained from $\langle\xi\rangle$ and $\langle\Gamma_{\mathrm{A}}\rangle$ by using Eqs. (7) and (8) as follows:

$$\langle\Gamma_{\mathrm{R}}\rangle = \langle\xi\rangle\Gamma_{\mathrm{A0}} - \langle\Gamma_{\mathrm{A}}\rangle, \tag{36}$$

$$\langle\Gamma_{\mathrm{B}}\rangle = (1 - \langle\xi\rangle)\Gamma_{\mathrm{B0}} - \langle\Gamma_{\mathrm{R}}\rangle. \tag{37}$$

In the self-similar region of the planar jet, the molecular diffusion term and the streamwise turbulent diffusion term can be neglected.[35] When these terms are neglected and the gradient diffusion model[2] is used for the turbulent mass flux, Eqs. (34) and (35) reduce to

$$\frac{\partial\langle\xi\rangle}{\partial x} = \frac{1}{\langle U\rangle}\left[-\langle V\rangle\frac{\partial\langle\xi\rangle}{\partial y} + \frac{\partial}{\partial y}\left(\frac{\nu_{\mathrm{T}}}{Sc_{\mathrm{T}}}\frac{\partial\langle\xi\rangle}{\partial y}\right)\right], \tag{38}$$

$$\frac{\partial\langle\Gamma_{\mathrm{A}}\rangle}{\partial x} = \frac{1}{\langle U\rangle}\left[-\langle V\rangle\frac{\partial\langle\Gamma_{\mathrm{A}}\rangle}{\partial y} + \frac{\partial}{\partial y}\left(\frac{\nu_{\mathrm{T}}}{Sc_{\mathrm{T}}}\frac{\partial\langle\Gamma_{\mathrm{A}}\rangle}{\partial y}\right) - k\left(\langle\Gamma_{\mathrm{A}}\rangle\langle\Gamma_{\mathrm{B}}\rangle + \langle\gamma_{\mathrm{A}}\gamma_{\mathrm{B}}\rangle\right)\right]. \tag{39}$$

Here, ν_{T} is the eddy viscosity and Sc_{T} is the turbulent Schmidt number, which is the model parameter of the gradient diffusion model. In a round jet, Yimer et al.[36] measured Sc_{T}, and showed that Sc_{T} has a value of $0.6 \sim 1.1$ in a self-similar region. Although the planar jet is considered here, we use a global constant $Sc_{\mathrm{T}} = 0.52$ in the numerical simulation. It has been reported that the eddy diffusivity (given by $\nu_{\mathrm{T}}/Sc_{\mathrm{T}}$) can change with chemical reactions[3–6] even if the heat release and the change in density by reactions can be neglected.

However, the change in the eddy diffusivity by chemical reactions is often neglected as in Wang and Tarbell[7]. We also use $Sc_{\mathrm{T}} = 0.52$ for both mixture fraction (nonreactive scalar) and concentration of the reactant A. When the eddy viscosity is assumed to be independent of the cross-streamwise direction in the self-similar region of the planar jet, ν_{T} in the self-similar region is represented by the following equation.[35]

$$\nu_{\mathrm{T}}(x,y) = \left[\ln\left(1+\sqrt{2}\right)^2\right]^{-2} \frac{db_U}{dx}\langle U\rangle_{\mathrm{C}} b_U, \tag{40}$$

If the mean velocity profiles $\langle U\rangle$ and $\langle V\rangle$ are known and the concentration correlation $\langle \gamma_{\mathrm{A}}\gamma_{\mathrm{B}}\rangle$ is modeled, Eqs. (38) and (39) can be numerically integrated in the x direction. Therefore, when cross-streamwise profiles of $\langle\xi\rangle$ and $\langle \Gamma_{\mathrm{A}}\rangle$ at any streamwise location in the self-similar region are given, the cross-streamwise profiles of $\langle\xi\rangle$ and $\langle \Gamma_{\mathrm{A}}\rangle$ in the further downstream region can be obtained from Eqs. (38) and (39).

In the numerical simulation carried out here, the mean concentrations in the region of $x/d \geq 10$ are predicted from the cross-streamwise profiles of the mean concentrations at $x/d = 10$ by using Eqs. (38) and (39). In this numerical simulation, the measurement results of the mean streamwise velocity and the mixture fraction variance are used for computing the mean velocity field and the mixture fraction variance. The mixture fraction variance is required in the Toor's model and the 3E model. The profiles of the mean velocity and the mixture fraction variance used in the simulation are shown later. The two-dimensional computational domain is the region of $10 \leq x/d \leq 42$ and $-25 \leq y/d \leq 25$, where the self-similar profile can be observed for the mean streamwise velocity and the mean mixture fraction (Figs. 3 and 4). The integers i and j are used for denoting the location of the computational grid in the x and y directions ($i = 1 \sim N_x$ and $j = 1 \sim N_y$). $i = 1$ and N_x correspond to $x/d = 10$ and 42, respectively, and $j = 1$ and N_y correspond to $y/d = -25$ and 25, respectively. Here, $N_x \times N_y = 4000 \times 300$ grid points are used in this simulation. The size of the computational grid is uniform in x and y directions. The x direction derivative in Eqs. (38) and (39) is approximated by

$$\left[\frac{\partial f}{\partial x}\right]_{i,j} = \frac{f_{i+1,j} - f_{i,j}}{\Delta x} \tag{41}$$

Here, Δx is the size of the computational grid in the x direction, and $f_{i,j}$ is the value of f at the computational grid point corresponding to (i,j). Then, $\langle\xi\rangle_{i+1,j}$ and $\langle \Gamma_{\mathrm{A}}\rangle_{i+1,j}$ can be

computed from the variables at the streamwise location of i as follows:

$$\langle \xi \rangle_{i+1,j} = \langle \xi \rangle_{i,j} + \frac{\Delta x}{\langle U \rangle_{i,j}} \left[-\langle V \rangle \frac{\partial \langle \xi \rangle}{\partial y} + \frac{\partial}{\partial y} \left(\frac{\nu_{\mathrm{T}}}{Sc_{\mathrm{T}}} \frac{\partial \langle \xi \rangle}{\partial y} \right) \right]_{i,j}, \tag{42}$$

$$\langle \Gamma_{\mathrm{A}} \rangle_{i+1,j} = \langle \Gamma_{\mathrm{A}} \rangle_{i,j} + \frac{\Delta x}{\langle U \rangle_{i,j}} \left[-\langle V \rangle \frac{\partial \langle \Gamma_{\mathrm{A}} \rangle}{\partial y} + \frac{\partial}{\partial y} \left(\frac{\nu_{\mathrm{T}}}{Sc_{\mathrm{T}}} \frac{\partial \langle \Gamma_{\mathrm{A}} \rangle}{\partial y} \right) - k \left(\langle \Gamma_{\mathrm{A}} \rangle \langle \Gamma_{\mathrm{B}} \rangle + \langle \gamma_{\mathrm{A}} \gamma_{\mathrm{B}} \rangle \right) \right]_{i,j}. \tag{43}$$

The right hand sides in Eqs. (42) and (43) are evaluated at the streamwise location of i. The y direction derivative is computed by using the second-order finite difference:

$$\left[\frac{\partial f}{\partial y} \right]_{i,j} = \frac{f_{i,j+1} - f_{i,j-1}}{2\Delta y}. \tag{44}$$

Here, Δy is the size of the computational grid in the y direction.

The concentration correlation $\langle \gamma_{\mathrm{A}} \gamma_{\mathrm{B}} \rangle$ in Eq. (43) is modeled by the Toor's model (Eq. (31)) or the 3E model (Eq. (33)). In Eqs. (31) and (33), the mixture fraction variance $\langle \xi'^2 \rangle$ is calculated by using the experimental results, whereas the mean mixture fraction and the mean concentration in Eqs. (31) and (33) are obtained by solving Eqs. (42) and (43).

The velocity and mixture fraction statistics used in the simulation

The profiles of the mean velocity and the mixture fraction variance in the computational domain are required for solving Eqs. (42) and (43). The mean characteristics of the streamwise velocity and the mixture fraction are shown in Figs. 3, 4, and 5. As shown in Fig. 3(b), the mean streamwise velocity profiles in the self-similar region can be approximated by using the Gaussian distribution[27]:

$$\langle U \rangle - U_{\mathrm{M}} = (\langle U \rangle_{\mathrm{C}} - U_{\mathrm{M}}) \exp \left[-\ln 2 (y/b_U)^2 \right] \tag{45}$$

We use the experimental values of $\langle U \rangle_{\mathrm{C}}$ and b_U for computing the mean streamwise velocity. $\langle U \rangle_{\mathrm{C}}$ and b_U in the self-similar region are given by Eqs. (15) and (16), in which the coefficients are determined from the experimental results. In the numerical simulation, the mean streamwise velocity $\langle U \rangle$ is calculated by using Eqs. (15), (16), and (45). In the planar jet, the averaged continuity equation is given by

$$\frac{\partial \langle U \rangle}{\partial x} + \frac{\partial \langle V \rangle}{\partial y} = 0. \tag{46}$$

In the planar jet, $\langle V \rangle$ is zero at $y = 0$ because the planar jet is statistically symmetrical with respect to the x-axis ($y = 0$). Therefore, when the mean streamwise velocity profile $\langle U \rangle$ is known, the profile of the mean cross-streamwise velocity $\langle V \rangle$ can be obtained by integrating Eq. (46) in the y direction.

The mixture fraction variance $\langle \xi'^2 \rangle = \xi_{\rm rms}^2$ in the self-similar region is calculated using the experimental values of $\xi_{\rm rms}$. Here, $\xi_{\rm rms}$ is the rms value of the mixture fraction fluctuation. In the self-similar region in the planar jet, $\xi_{\rm rms}$ can be represented by

$$\xi_{\rm rms} = \xi_{\rm rmsC} f_\xi(y/b_\xi). \tag{47}$$

Here, $\xi_{\rm rmsC}$ is $\xi_{\rm rms}$ on the jet centerline and $f_\xi(y/b_\xi)$ is the self-similar profile for $\xi_{\rm rms}$. The profiles of $\xi_{\rm rmsC}$, b_ξ, and $f_\xi(y/b_\xi)$ are obtained from the experimental results. The jet half-width b_ξ is calculated by using Eq. (17) in the self-similar region. Figures 21(a) and (b) show $\xi_{\rm rmsC}$ and $\xi_{\rm rms}/\xi_{\rm rmsC} = f_\xi(y/b_\xi)$, respectively. The solid red curve in Fig. 21(a) is obtained by applying the least-square method. Similarly, the solid red curve in Fig. 21(b) is obtained by applying the least-square method to the cross-streamwise profile of $\xi_{\rm rms}$ at $x/d = 20$. Here, the fifth-order functions of x/d and y/b_ξ are used to approximate $\xi_{\rm rmsC}$ and $f_\xi(y/b_\xi)$, respectively. These curves obtained by the least-square method are used to calculate $\xi_{\rm rms}$ in the computational domain by using Eq. (47).

Boundary condition for the mean concentrations

At $y = -L_y/2$ and $y = L_y/2$, the y direction gradient of the mean concentrations is set to zero. The cross-streamwise profiles of the mean concentrations at $x/d = 10$ are determined from the experimental results. Figure 22 shows the cross-streamwise profiles of $\langle \xi \rangle$ and $\langle \mathit{\Gamma}_{\rm A} \rangle$ at $x/d = 10$. Because the statistics in the planar jet are symmetrical with respect to the x-axis, the region of $y \geq 0$ is shown in Fig. 22. The solid lines in Fig. 22, which are obtained by applying the least-square method, are used as the boundary condition in the numerical simulation. Because the mean concentration of the species A in the nonreactive case is represented by $\langle \mathit{\Gamma}_{\rm A} \rangle = \langle \xi \rangle \mathit{\Gamma}_{\rm A0}$, the mean mixture fraction profile shows the mean concentration profile of the species A in the nonreactive flow. The mean mixture fraction and the mean concentrations in the computational domain are computed by using Eqs. (42) and (43) and the profiles of $\langle \xi \rangle$ and $\langle \mathit{\Gamma}_{\rm A} \rangle$ at $x/d = 10$.

Mean concentration profiles predicted by the averaged transport equation using Toor's model or 3E model

Figure 23 compares the jet half-width based on the mean mixture fraction between the experiment and the numerical simulation. In the numerical simulation, the jet development strongly depends on the turbulent Schmidt number Sc_{T}. The jet half-width obtained by the numerical simulation agrees well with the experimental values. Thus, it is found that the mean mixture fraction development is well predicted by the numerical simulation.

The mean concentration profile of the reactant A is compared between the experiment and the numerical simulation using the Toor's model or the 3E model. Figures 24(a) and (b) compare the cross-streamwise profiles of the mean concentration of A, $\langle \mathit{\Gamma}_{\mathrm{A}} \rangle$, at $x/d = 20$ and 40 between the experiment and the numerical simulation for the nonreactive case (frozen limit, $Da = 0$) and the reactive case with the finite Damköhler number ($Da = 11.7$). In the nonreactive case, $\langle \mathit{\Gamma}_{\mathrm{A}} \rangle$ obtained by the numerical simulation near the jet centerline ($y/b_\xi \leq 1$) agrees well with the experiment. At the edge of the jet, $\langle \mathit{\Gamma}_{\mathrm{A}} \rangle$ in the nonreactive case is overestimated by the numerical simulation. In the numerical simulation, the eddy viscosity ν_{T} is assumed to be independent of the cross-streamwise (y) direction. In fact, the eddy diffusivity in jet flows changes in the y direction. It is known that when the dependence of ν_{T} on the y direction is neglected in RANS simulations of jets, the mean streamwise velocity and the mean concentration profiles are poorly predicted at the edge of jets by the numerical simulation.[35] The inconsistence in the mean concentration at the edge between the experiment and the numerical simulation is expected to arise from the assumption that the eddy diffusivity is independent of the y direction.

The mean concentration profile $\langle \mathit{\Gamma}_{\mathrm{A}} \rangle$ in the reactive case is compared between the experiment and the numerical simulation near the jet centerline ($|y/b_\xi| \leq 1$), where $\langle \mathit{\Gamma}_{\mathrm{A}} \rangle$ in the nonreactive case is well predicted by the numerical simulation. In the region of $|y/b_\xi| \leq 1$, $\langle \mathit{\Gamma}_{\mathrm{A}} \rangle$ obtained by the simulation is smaller than experimental values for both the Toor's model and the 3E model. Thus, the chemical consumption of the reactant A is overestimated by the numerical simulation. The mean reaction rate is given by Eq. (3). The experimental results in Fig. 19 show that the concentration correlation predicted by the Toor's model is small in magnitude compared with the experimental values. From Fig. 19(b), it is also found that the concentration correlation predicted by the 3E model is also

small in magnitude at $x/d = 20$. Not only at $x/d = 20$ but also at $x/d = 40$ (Fig. 19(c)), the concentration correlation predicted by the Toor's model or the 3E model is different from the experimental values. However, because the reactive species are transported towards the downstream region, the discrepancy in the concentration correlation in the upstream region has a greater influence on the mean concentration profile in the downstream region. Because the concentration correlation $\langle \gamma_A \gamma_B \rangle$ is negative and the mean chemical reaction rate $\langle W \rangle$ is positive, Eq. (3) shows that the underpredicted $\langle \gamma_A \gamma_B \rangle$ results in the large mean reaction rate. The small mean concentration of the reactant A obtained by the numerical simulation in this study can be related to the overestimation of the mean reaction rate by the Toor's model and the 3E model. Thus, when the Toor's model or the 3E model is used for the concentration correlation, the effect of the chemical reaction on the mean concentrations is overestimated in the numerical simulation using the averaged transport equation for the concentrations of reactive species.

CONCLUSIONS

Instantaneous concentrations of reactive species were simultaneously measured in a planar liquid jet with a second-order chemical reaction A + B $\rightarrow$ R in order to investigate the statistical properties of the chemical reaction rate and the validity of the models for the concentration correlation. The reactant A was premixed in the jet flow, and the reactant B was premixed in the ambient flow.

First, we investigated the statistical properties of the chemical reaction rate in the planar liquid jet. The measurement of the mean reaction rate shows that the second-order chemical reaction mainly occurs near the jet centerline in the upstream region. The concentration correlation of the reactants A and B makes a negative contribution to the mean reaction rate. A comparison between the mean reaction rate and the concentration correlation shows that the contribution of concentration correlation to the mean reaction rate becomes important in the downstream direction. The chemical reaction increases the magnitude of the concentration correlation $\langle \gamma_A \gamma_B \rangle$ for $Da = 11.7$ in the outer part of the upstream region. In the other regions, $\langle \gamma_A \gamma_B \rangle$ becomes small in magnitude because of the chemical reaction. However, the fast chemical reaction (i.e., large Da) reduces the concentration correlation magnitude throughout the entire jet region. The measurements of the concentration corre-

lation show that the effects of the chemical reaction on the concentration correlation change with location in the flow and the value of the Damköhler number. The cospectra of the concentrations of the reactants A and B show that the large scales, which contain most of the energy of velocity fluctuation, largely contribute to the concentration correlation in the planar jet. Therefore, the change in the large-scale fluctuations by the reaction makes the difference in the concentration correlation between the reactive and nonreactive cases.

The concentration correlations predicted by the Toor's model and the 3E model are compared with the experimental results in order to investigate the validity of these models. The results show that the concentration correlation predicted by the Toor's model is small in magnitude compared with the experimental results, and the 3E model also fails to accurately estimate the concentration correlation in the region where the concentration correlation is largely affected by the chemical reaction. The 3E model well predicts the concentration correlation for the case in which the change of concentration correlation caused by the chemical reaction is small. To further investigate the validity of the models for the concentration correlation, the numerical simulation of the reactive planar liquid jet was performed by using the averaged transport equations for the mixture fraction and the concentration of the reactant A. The Toor's model or the 3E model was used in this simulation. The numerical results show that the effect of the chemical reaction on the mean concentrations is overestimated in the numerical simulation using the Toor's model or the 3E model. It is concluded that both the Toor's model and the 3E model are inadequate for modeling chemical reactions in a liquid jet. The measurement results in this paper will be useful to validate other numerical methods for modeling turbulent reactive flows at high Schmidt number.

ACKNOWLEDGMENTS

The authors would like to thank Dr. Takashi Kubo (Meijo University) and Mr. Takahiro Naito (Nagoya University) for their help in this study. KN acknowledges Prof. Satoru Komori (Kyoto University) for providing the key idea of this study and many valuable comments. The authors also acknowledge anonymous referees for valuable comments. This work was supported by JSPS KAKENHI Grant Number 25002531 and MEXT KAKENHI Grant Numbers 25289030, 25289031, and 25630052.

REFERENCES

[1]Fox RO. Computational models for turbulent reacting flows. Cambridge Univ Pr., 2003.

[2]Combest DP, Ramachandran PA, Dudukovic MP. On the gradient diffusion hypothesis and passive scalar transport in turbulent flows. Ind Eng Chem Res. 2011;50:8817–8823.

[3]Bilger RW, Saetran LR, Krishnamoorthy LV. Reaction in a scalar mixing layer. J Fluid Mech. 1991;233:211–242.

[4]Toor HL. Effect of chemical reactions on turbulent diffusivities. AIChE J. 1993;39:1603–1610.

[5]Komori S, Nagata K, Kanzaki T, Murakami Y. Measurements of mass flux in a turbulent liquid flow with a chemical reaction. AIChE J. 1993;39:1611–1620.

[6]Watanabe T, Sakai Y, Nagata K, Terashima O. Turbulent Schmidt number and eddy diffusivity change with a chemical reaction. J Fluid Mech. 2014;754:98–121.

[7]Wang DM, Tarbell JM. Closure models for turbulent reacting flows with a nonhomogeneous concentration field. Chem Eng Sci. 1993;48:3907–3920.

[8]Veynante D, Vervisch L. Turbulent combustion modeling. Prog Energy Combust Sci. 2002;28:193–266.

[9]Brown RJ, Bilger RW. An experimental study of a reactive plume in grid turbulence. J Fluid Mech. 1991;312:373–407.

[10]de Bruyn Kops SM, Riley JJ, Kosaly G. Direct numerical simulation of reacting scalar mixing layers. Phys Fluids. 2001;13:1450.

[11]Fabregat A, Pallarès J, Cuesta I, Grau FX. Numerical simulations of a second-order chemical reaction in a plane turbulent channel flow. Int J Heat Mass Transfer. 2010;53:4248–4263.

[12]Komori S, Kanzaki T, Murakami Y. Concentration correlation in a turbulent mixing layer with chemical reactions. J Chem Eng Jpn. 1994;27:742–748.

[13]Zhdanov V, Chorny A. Development of macro- and micromixing in confined flows of reactive fluids. Int J Heat Mass Transfer. 2011;54:3245–3255.

[14]Chorny A, Zhdanov V. Turbulent mixing and fast chemical reaction in the confined jet flow at large Schmidt number. Chem Eng Sci. 2012;68:541–554.

[15]Nakamura I, Sakai Y, Miyata M. Diffusion of matter by a non-buoyant plume in grid-generated turbulence. J Fluid Mech. 1987;178:379–403.

[16]Kubo T, Sakai Y, Nagata K, Iida K. Experimental study on the turbulent reactive plane

jet in liquid. J Fluid Sci Tech. 2009;4:368–378.

[17]Watanabe T, Sakai Y, Nagata K, Terashima O, Kubo T. Simultaneous measurements of reactive scalar and velocity in a planar liquid jet with a second-order chemical reaction. Exp Fluids. 2012;53:1369–1383.

[18]Kubo T, Fukumura Y, Sakai Y, Nagata K. Study on turbulent plane jet with chemical reaction in liquid. J Fluid Sci Tech. 2012;7:25–38.

[19]Watanabe T, Sakai Y, Nagata K, Terashima O. Joint statistics between velocity and reactive scalar in a turbulent liquid jet with a chemical reaction. Phys Scr. 2013;T155:014039.

[20]Naito T, Watanabe T, Sakai Y, Nagata K, Terashima O, Ito Y. Improvement of a spatial resolution of concentration measurement system based on the light absorption spectrometric method. Proceedings of the 4th International Conference on Jets, Wakes and Separated Flows (ICJWSF-2013). 2013;ICJWSF2013:1218.

[21]Naito T, Watanabe T, Sakai Y, Nagata K, Terashima O, Ito Y. Concentration measurement in a planar liquid jet with a chemical reaction by using the improved concentration measurement system based on the light absorption method. J. Fluid Sci. Technol. 2014 (accepted).

[22]Stanley SA, Sarkar S, Mellado JP. A study of the flow-field evolution and mixing in a planar turbulent jet using direct numerical simulation. J Fluid Mech. 2002;450:377–407.

[23]Klein M, Sadiki A, Janicka J. Investigation of the influence of the Reynolds number on a plane jet using direct numerical simulation. Int J Heat Fluid Flow. 2003;24:785–794.

[24]da Silva CB, Pereira JCF. Invariants of the velocity-gradient, rate-of-strain, and rate-of-rotation tensors across the turbulent/nonturbulent interface in jets. Phys Fluids. 2008;20:055101.

[25]Davies AE, Keffer JF, Baines WD. Spread of a heated plane turbulent jet. Phys Fluids. 1975;18:770–775.

[26]Browne LWB, Antonia RA, Chambers AJ. The interaction region of a turbulent plane jet. J Fluid Mech. 1984;149:355–373.

[27]Deo RC, Mi J, Nathan GJ. The influence of Reynolds number on a plane jet. Phys Fluids. 2008;20:075108.

[28]Bourne JR, Hilber C, Tovstiga G. Kinetics of the azo coupling reactions between 1-naphthol and diazotised sulphanilic acid. Chem Eng Commun. 1985;37:293–314.

[29]Gibson CH, Libby PA. On turbulent flows with fast chemical reactions. Part II. The distri-

bution of reactants and products near a reacting surface. Combust Sci Technol. 1972;6:29–35.

[30]Komori S, Hunt JCR, Kanzaki T, Murakami Y. The effects of turbulent mixing on the correlation between two species and on concentration fluctuations in non-premixed reacting flows. J Fluid Mech. 1991;228:629–659.

[31]Hill JC. Homogeneous turbulent mixing with chemical reaction. Annu Rev Fluid Mech. 1976;8:135–161.

[32]Toor HL. Turbulent mixing of two species with and without chemical reactions. Ind Eng Chem Fundam. 1969;8:655–659.

[33]Patterson GK. Application of turbulence fundamentals to reactor modelling and scaleup. Chem Eng Commun. 1981;8:25–52.

[34]Dutta A, Tarbell JM. Closure models for turbulent reacting flows. AIChE J. 1989;35:2013–2027.

[35]Pope SB. Turbulent flows. Cambridge Univ Pr., 2000.

[36]Yimer I, Campbell I, Jiang LY. Estimation of the turbulent Schmidt number from experimental profiles of axial velocity and concentration for high-Reynolds-number jet flows. Can Aeronaut Space J. 2002;48:195.

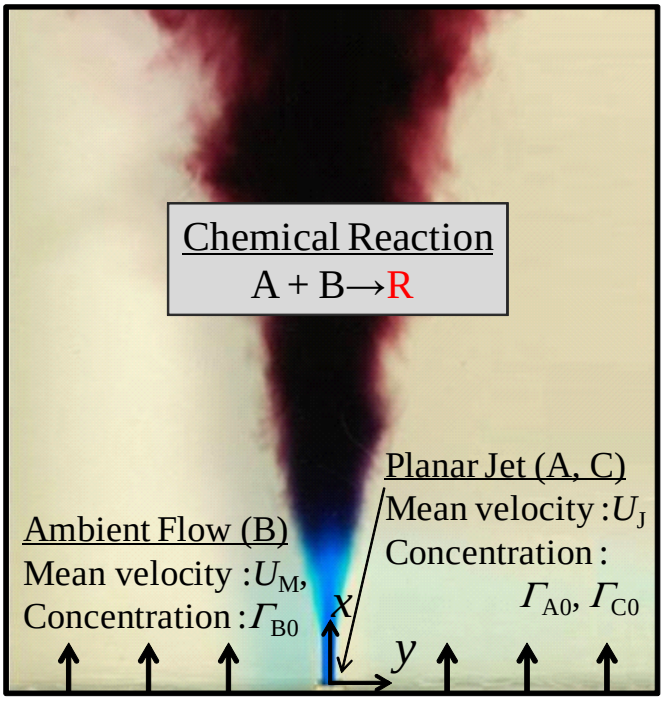

FIG. 1. Snapshot of a planar liquid jet with a chemical reaction.

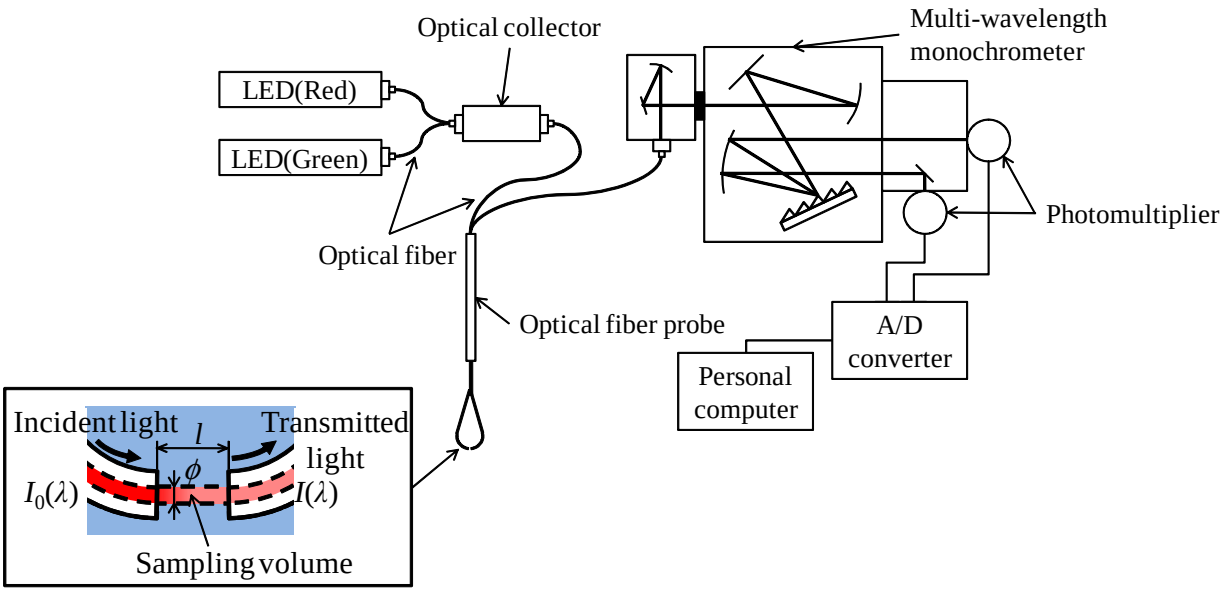

FIG. 2. Concentration measurement system based on light absorption spectrometry.

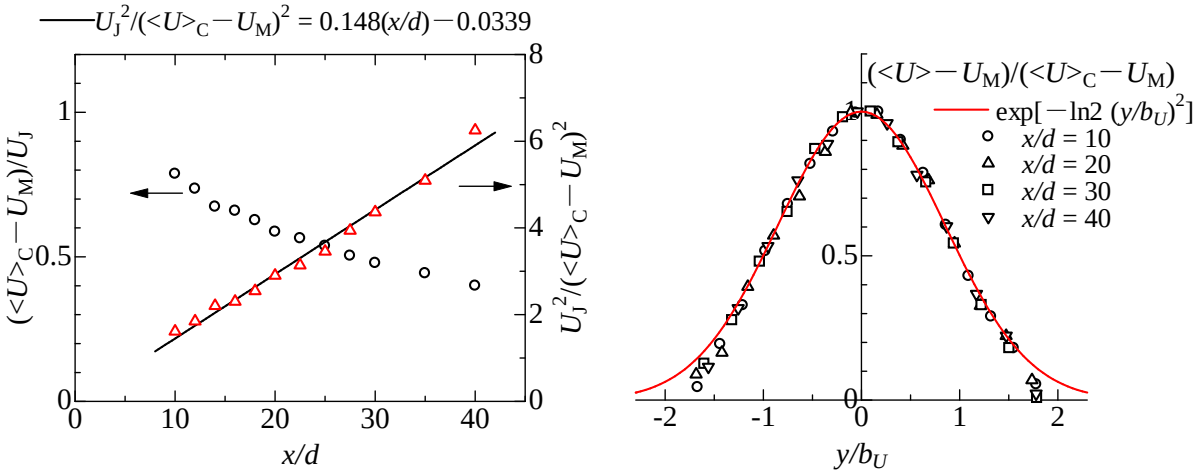

(a) Streamwise variation of the mean streamwise velocity on the jet centerline

(b) Cross-streamwise profiles of the mean streamwise velocity

FIG. 3. The mean streamwise velocity.

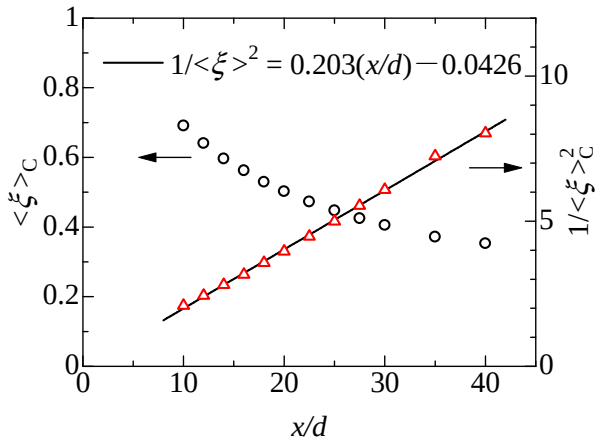

(a) Streamwise variation of the mean mixture fraction on the jet centerline

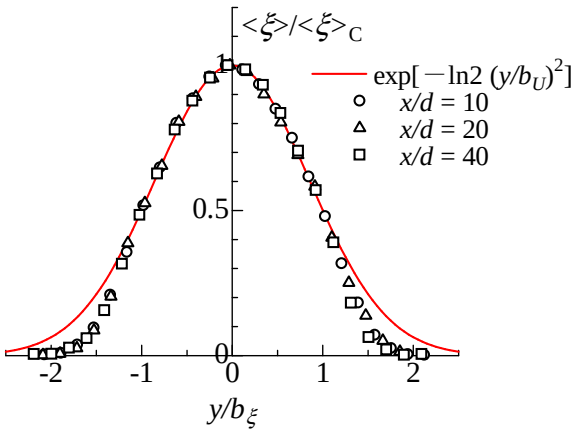

(b) Cross-streamwise profiles of the mean mixture fraction

FIG. 4. The mean mixture fraction.

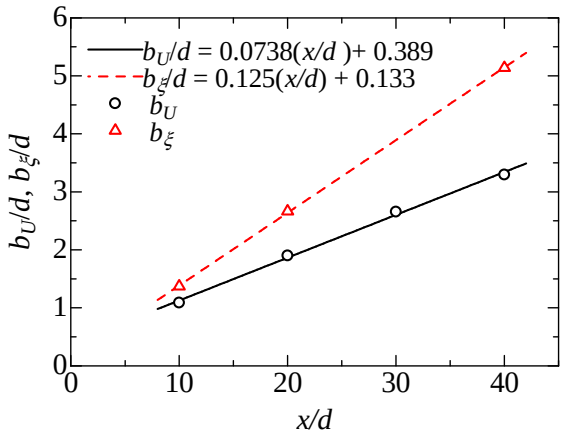

FIG. 5. Streamwise evolution of the jet half-widths based on the mean streamwise velocity and the mean mixture fraction.

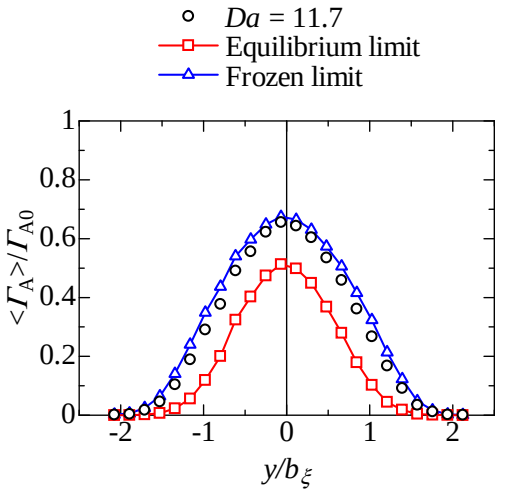

(a) $x/d = 10$

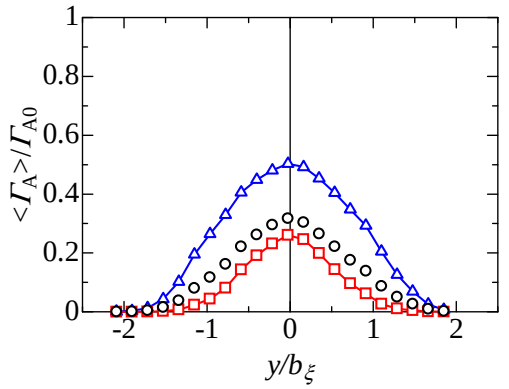

(b) $x/d = 20$

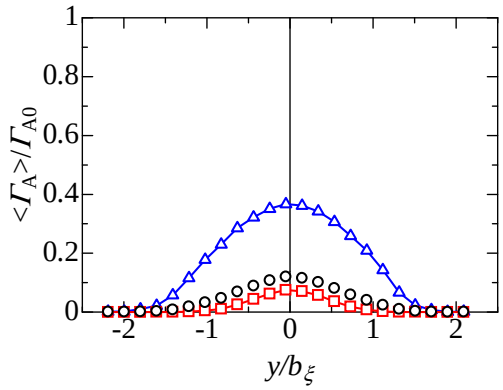

(c) $x/d = 40$

FIG. 6. Cross-streamwise profiles of the mean concentration of the reactant A.

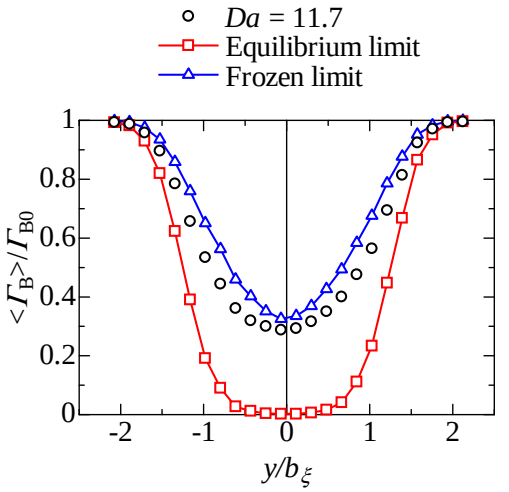

(a) $x/d = 10$

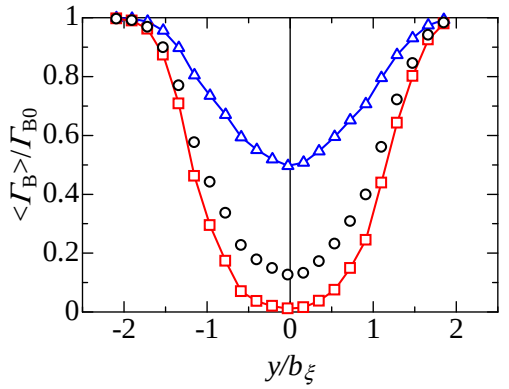

(b) $x/d = 20$

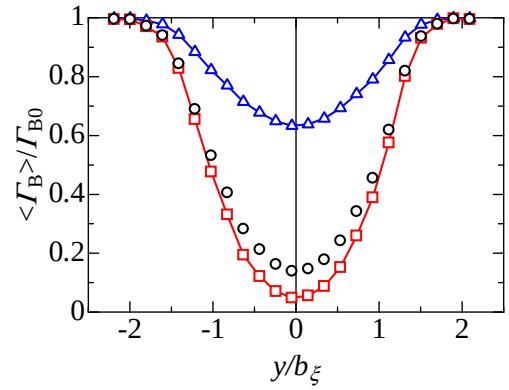

(c) $x/d = 40$

FIG. 7. Cross-streamwise profiles of the mean concentration of the reactant B.

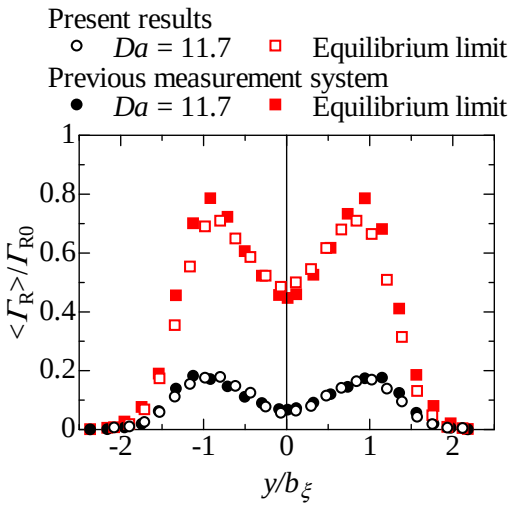

(a) $x/d = 10$

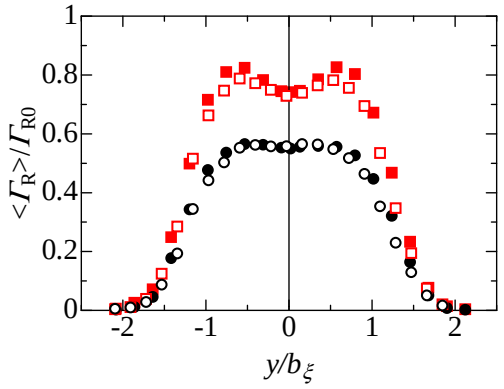

(b) $x/d = 20$

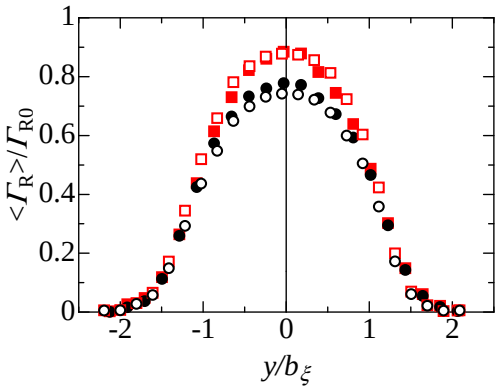

(c) $x/d = 40$

FIG. 8. Cross-streamwise profiles of the mean concentration of the product R. The present results are compared with the mean concentrations obtained by the previous concentration measurement system.[18]

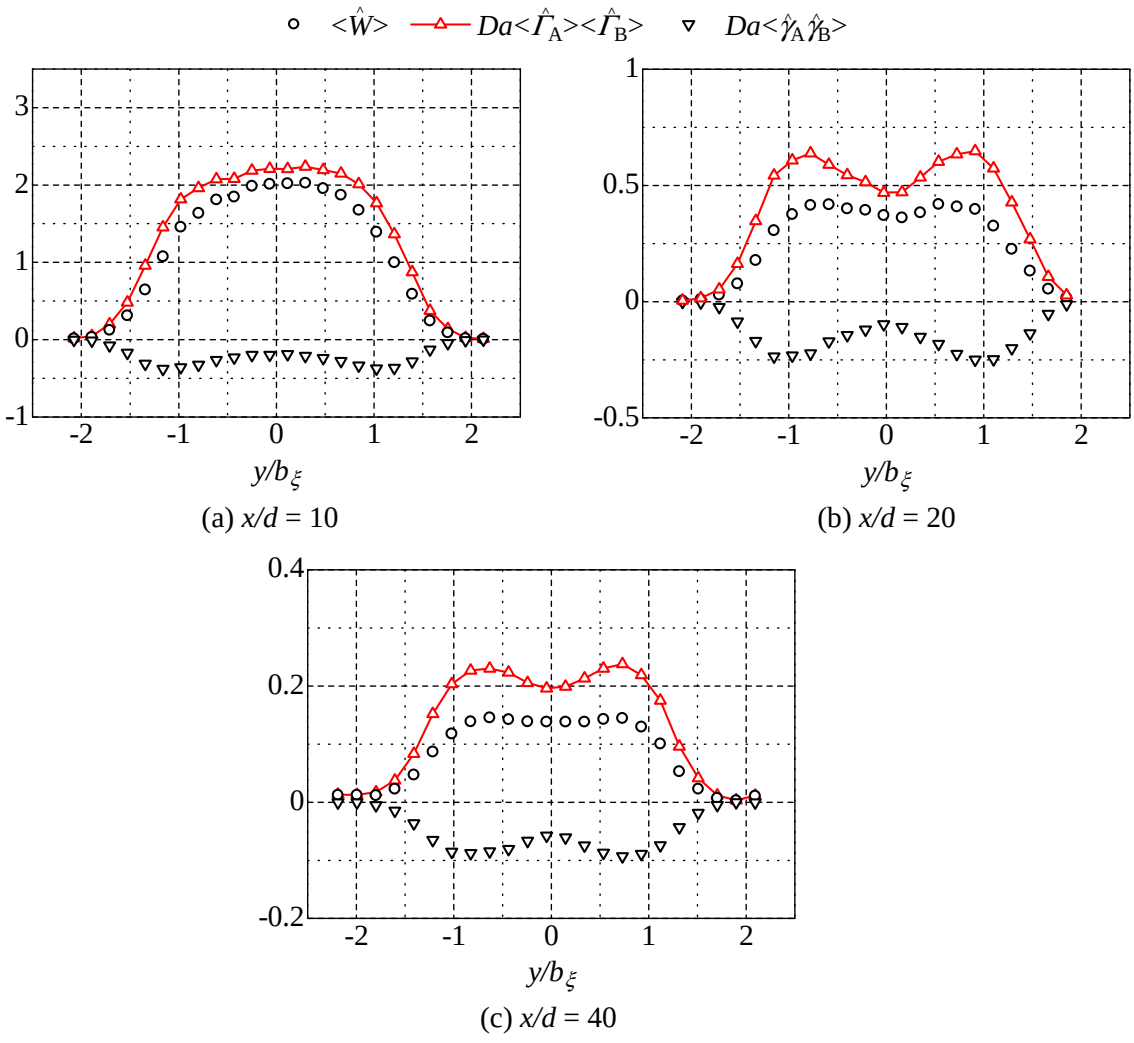

FIG. 9. Cross-streamwise profiles of the mean reaction rate.

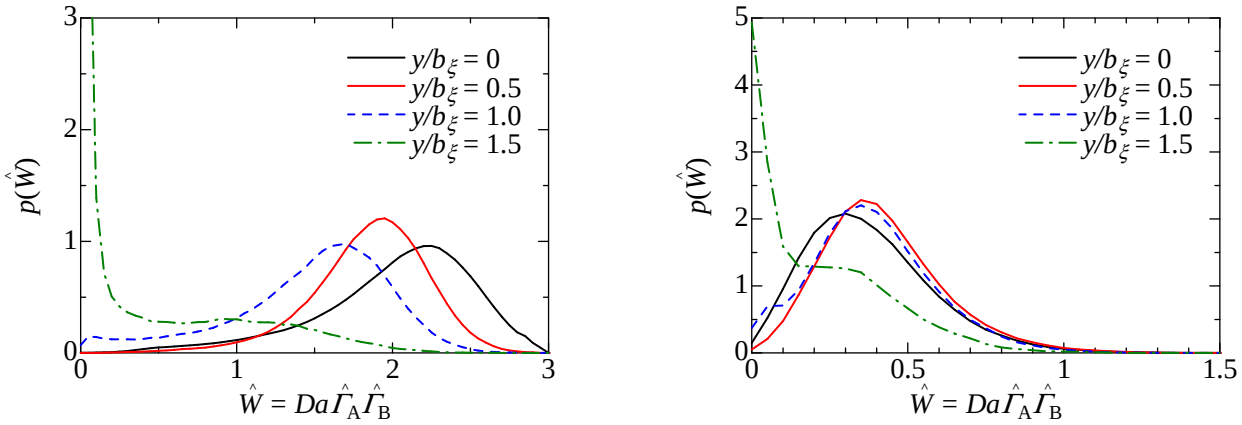

FIG. 10. Cross-streamwise variations of the probability density function of the reaction rate.

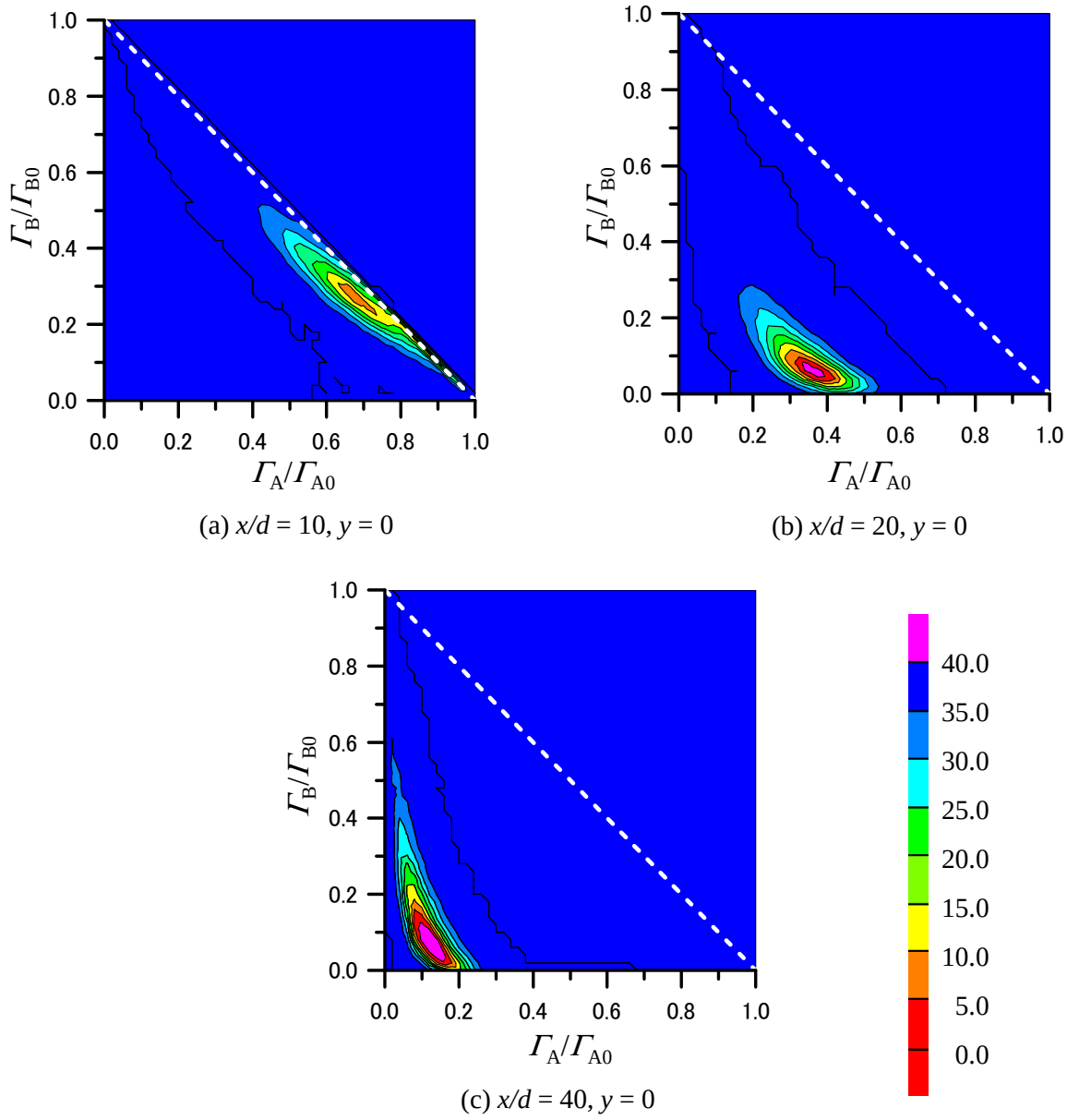

(a) $x/d = 10$, $y = 0$

(b) $x/d = 20$, $y = 0$

(c) $x/d = 40$, $y = 0$

FIG. 11. The joint probability density function of the concentrations of the reactants A and B on the jet centerline.

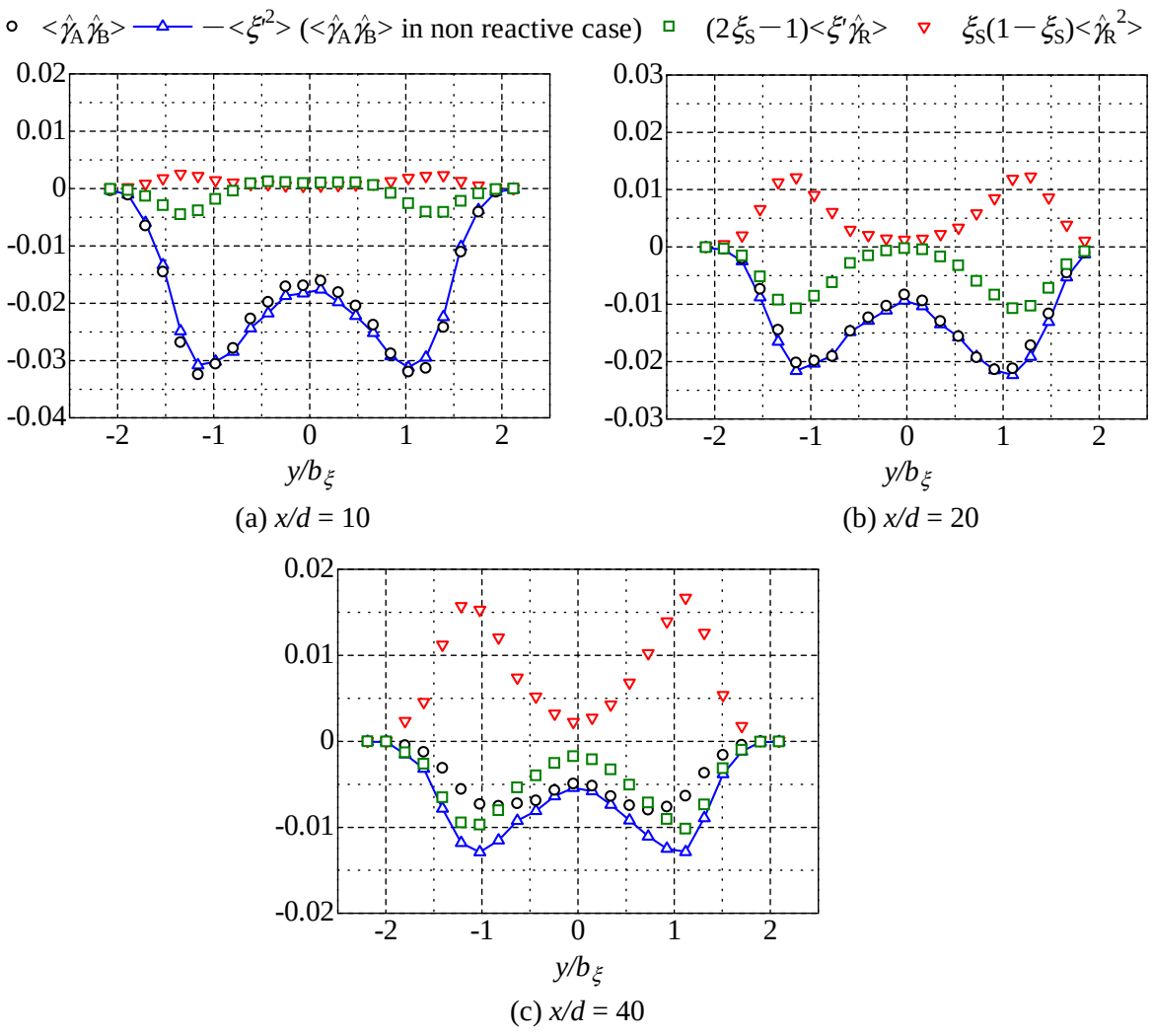

FIG. 12. Cross-streamwise profiles of the concentration correlation for $Da = 11.7$.

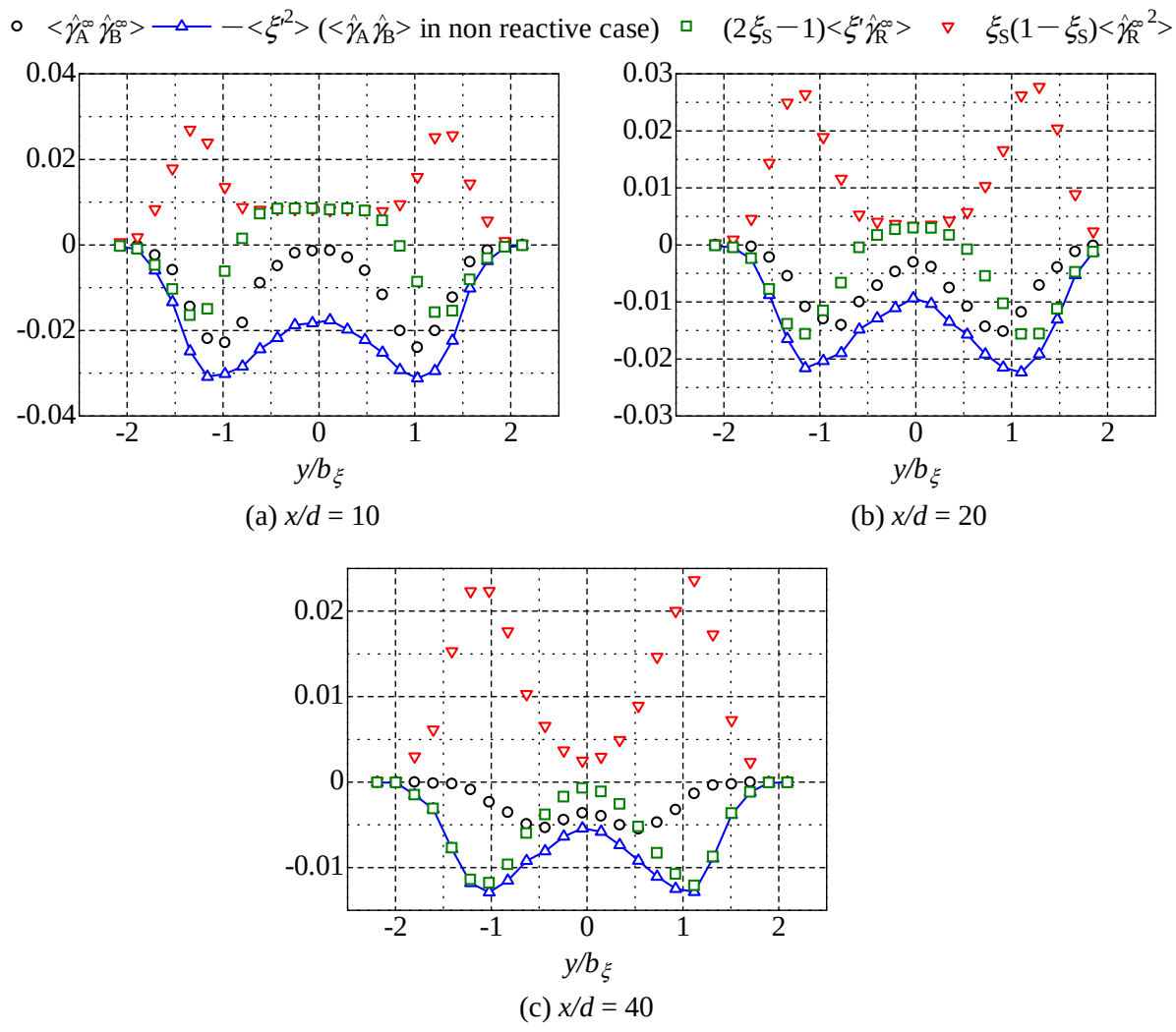

FIG. 13. Cross-streamwise profiles of the concentration correlation for the equilibrium limit.

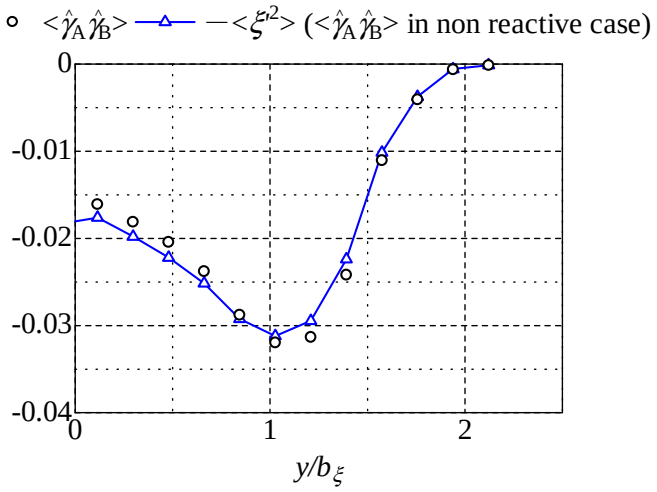

FIG. 14. Cross-streamwise profiles of the concentration correlation for $Da = 11.7$ at $x/d = 10$.

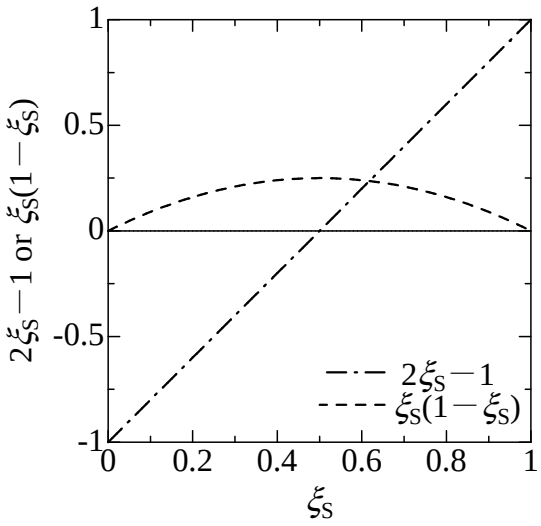

FIG. 15. Changes of $(2\xi_S - 1)$ and $\xi_S(1 - \xi_S)$ with ξ_S.

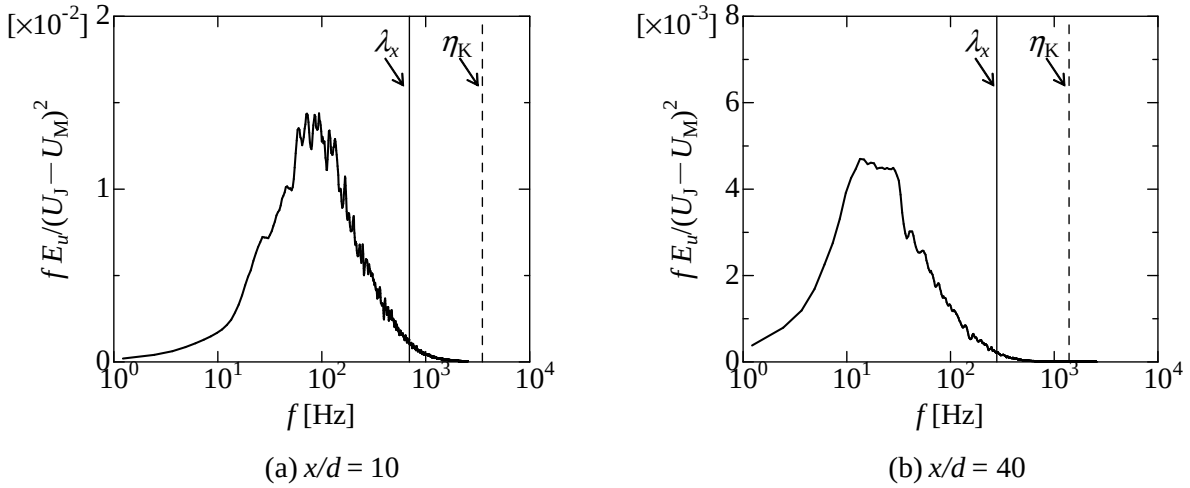

FIG. 16. Power spectra of the streamwise velocity at $x/d = 10$ and 40 on the jet centerline. The frequencies corresponding to the Taylor microscale λ_x and the Kolmogorov scale $\eta_{\rm K}$ are shown by the vertical solid and broken lines, respectively. The frequencies corresponding to λ_x and $\eta_{\rm K}$ are obtained by using the Taylor hypothesis of a frozen turbulence.

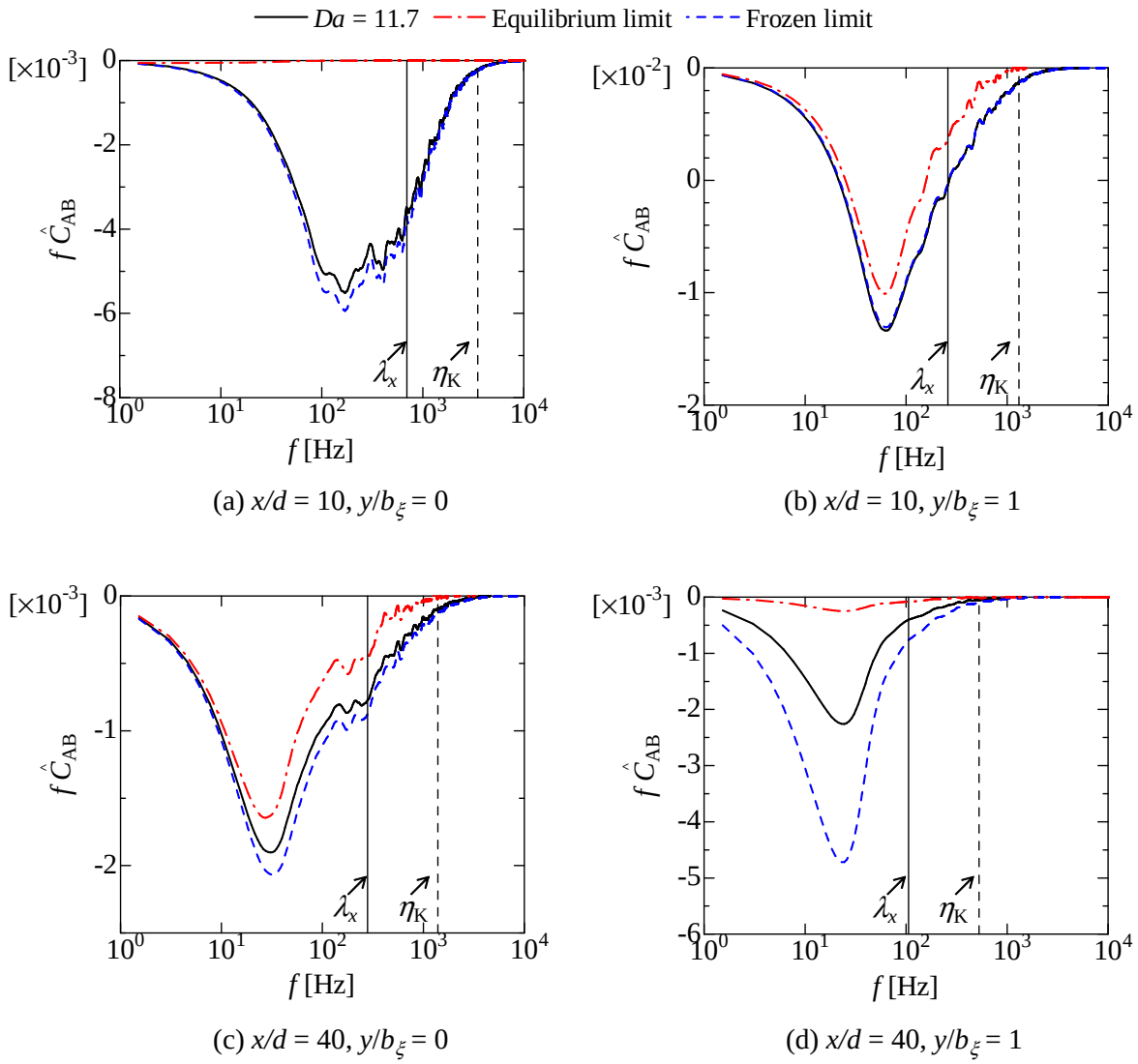

FIG. 17. Cospectra of the concentrations of the reactants A and B at four different locations. (a) $(x/d, y/b_\xi) = (10, 0)$. (b) $(x/d, y/b_\xi) = (10, 1)$. (c) $(x/d, y/b_\xi) = (40, 0)$. (d) $(x/d, y/b_\xi) = (40, 1)$. The cospectra for the frozen and equilibrium limits are also shown in this figure. The frequencies corresponding to the Taylor microscale λ_x and the Kolmogorov scale η_K are shown by the vertical solid and broken lines, respectively.

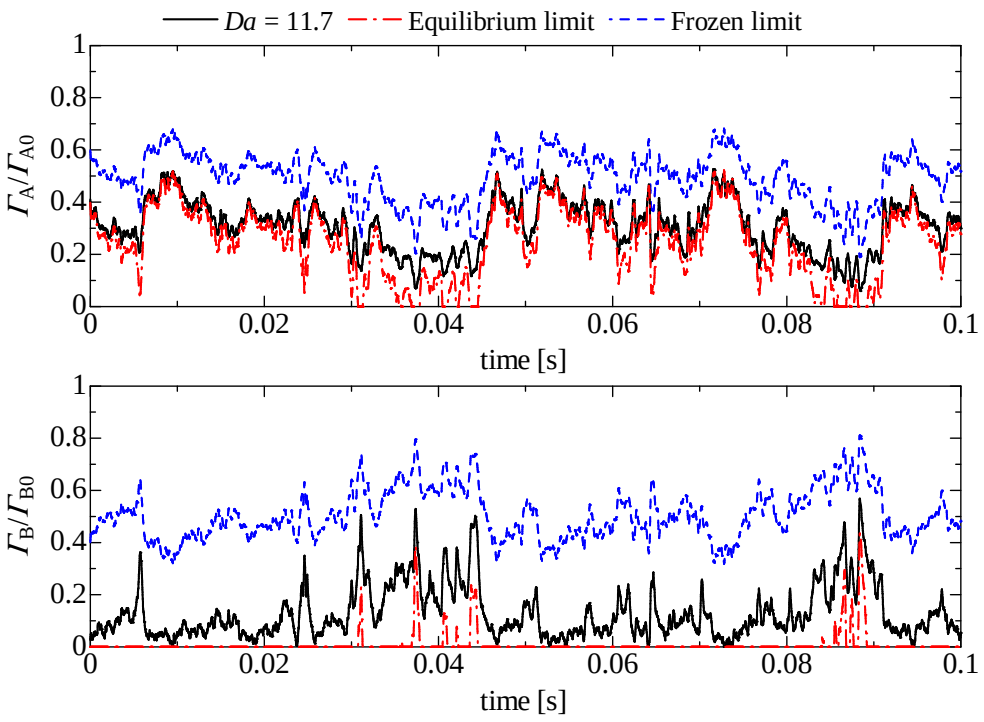

(a) $x/d = 20$, $y/b_\xi = 0$

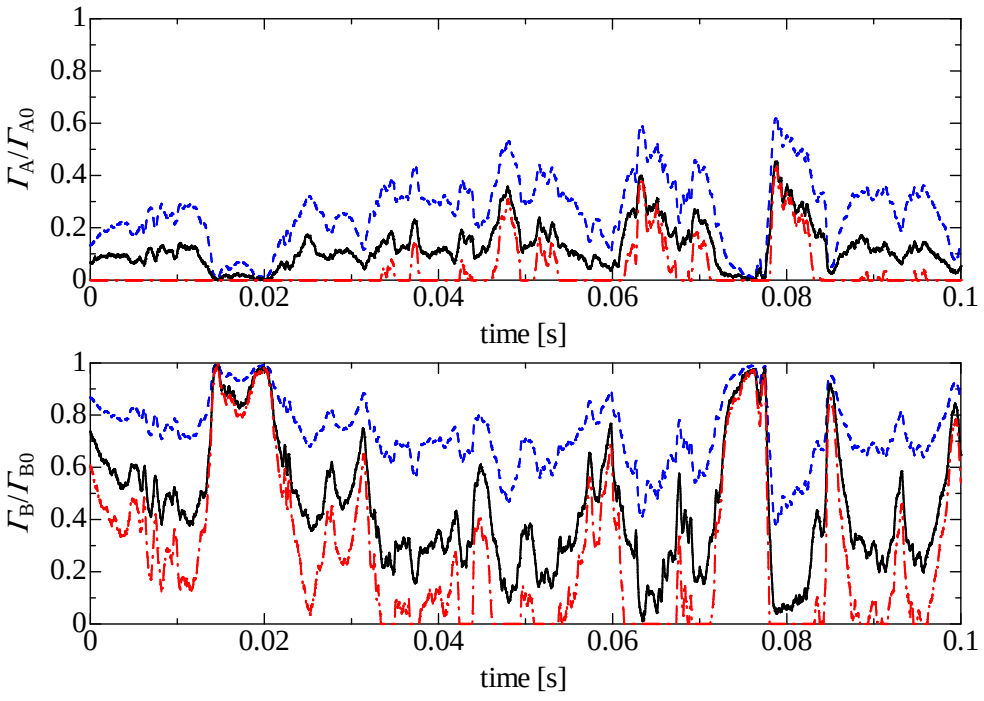

(b) $x/d = 20$, $y/b_\xi = 1$

FIG. 18. Instantaneous concentrations of the reactants A and B. (a) $(x/d, y/b_\xi) = (20, 0)$. (b) $(x/d, y/b_\xi) = (20, 1)$.

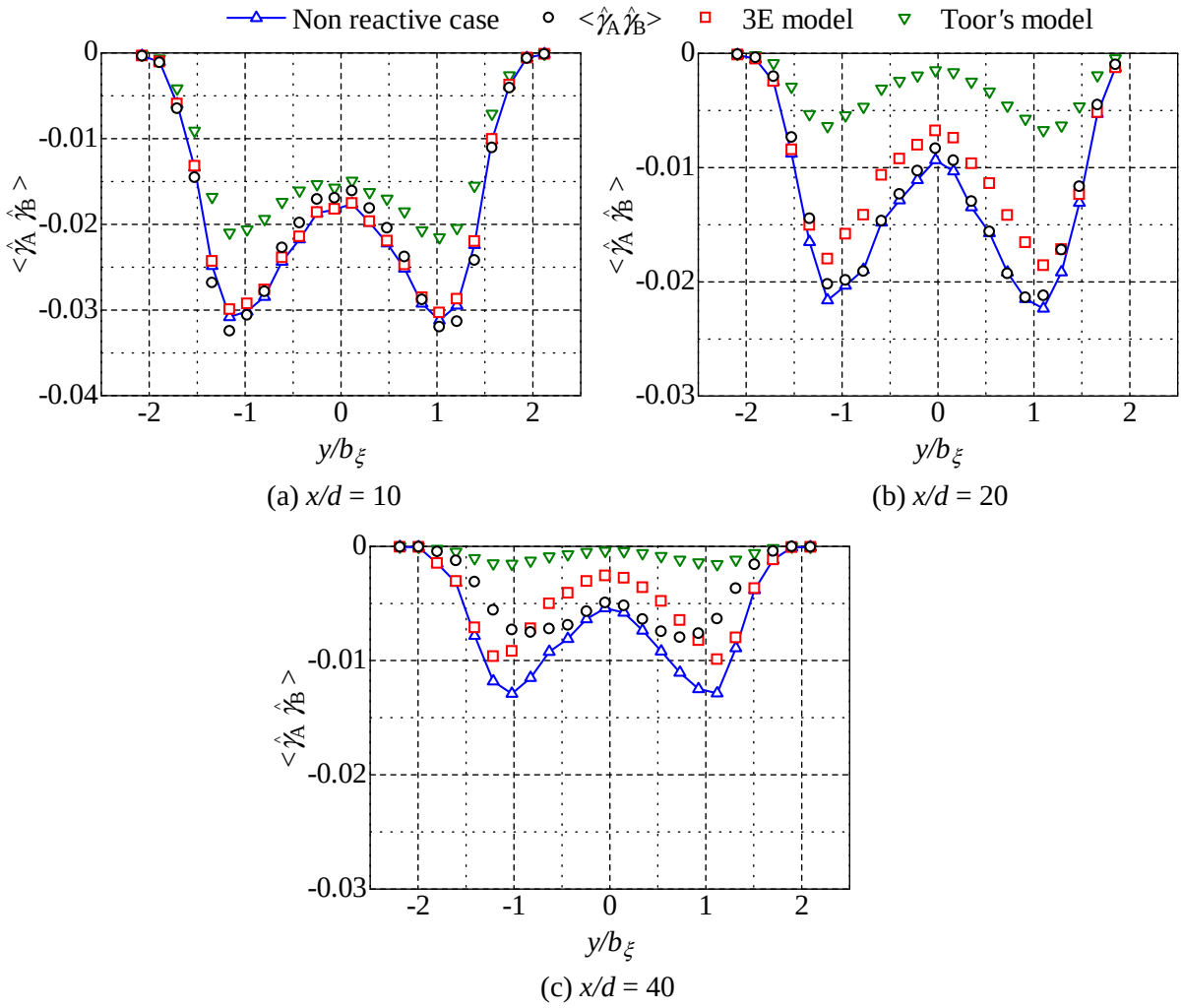

FIG. 19. Comparisons of the concentration correlation for $Da = 11.7$ between the measurement results and the models.

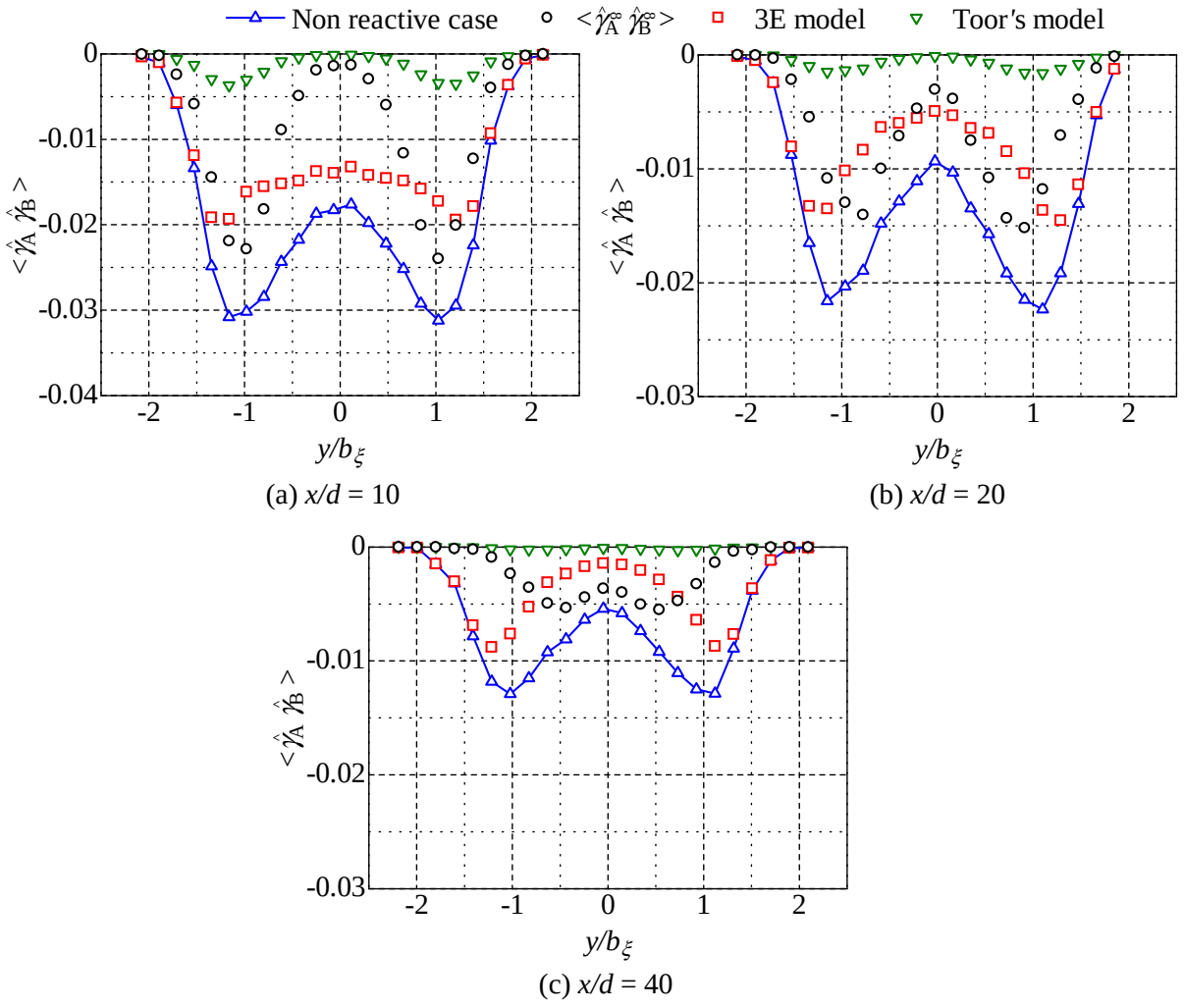

FIG. 20. Comparisons of the concentration correlation for the equilibrium limit between the measurement results and the models.

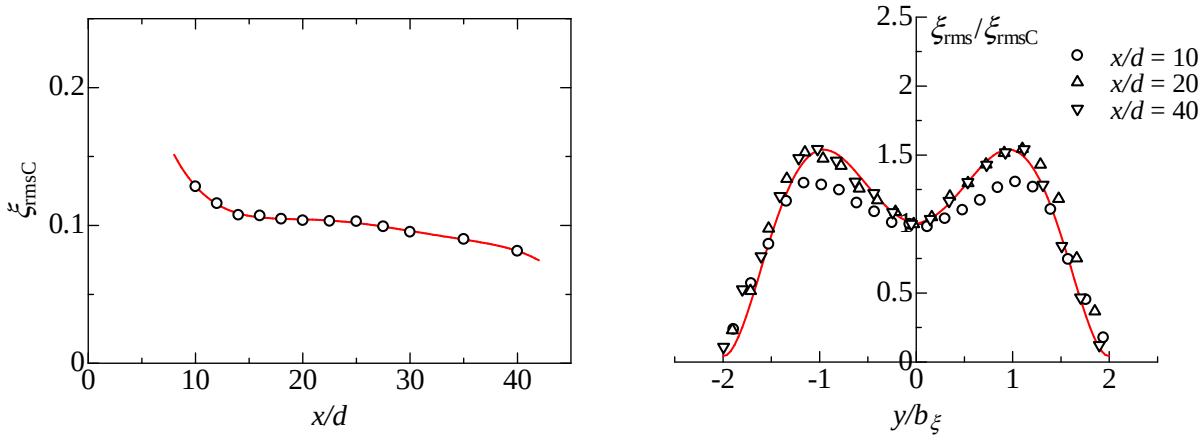

(a) Streamwise variation of the rms value of mixture fraction fluctuation on the jet centerline

(b) Cross-streamwise profiles of the rms value of mixture fraction fluctuation

FIG. 21. The rms value of mixture fraction fluctuation.

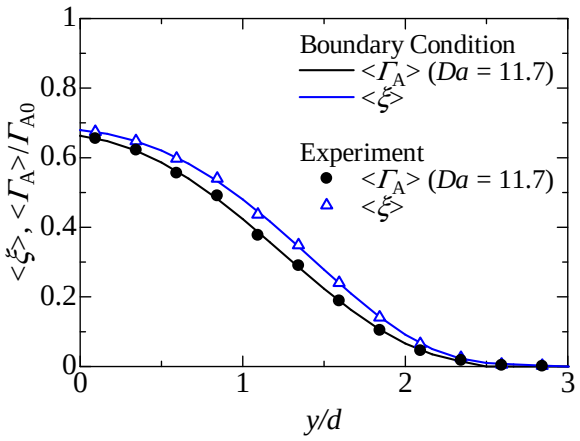

FIG. 22. Cross-streamwise profiles of the mean mixture fraction $\langle \xi \rangle$ and the mean concentration of the reactant A $\langle \Gamma_{\mathrm{A}} \rangle$ at $x/d = 10$. Cross-streamwise profiles of $\langle \xi \rangle$ and $\langle \Gamma_{\mathrm{A}} \rangle$ used as the boundary condition in the numerical simulation are shown by solid lines.

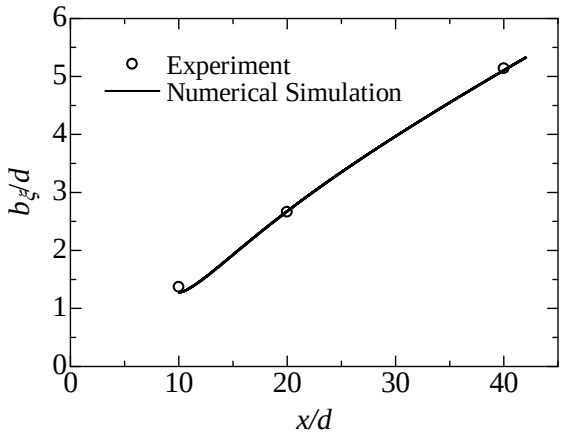

FIG. 23. Comparison of the jet half-width based on the mean mixture fraction between the experiment and the numerical simulation.

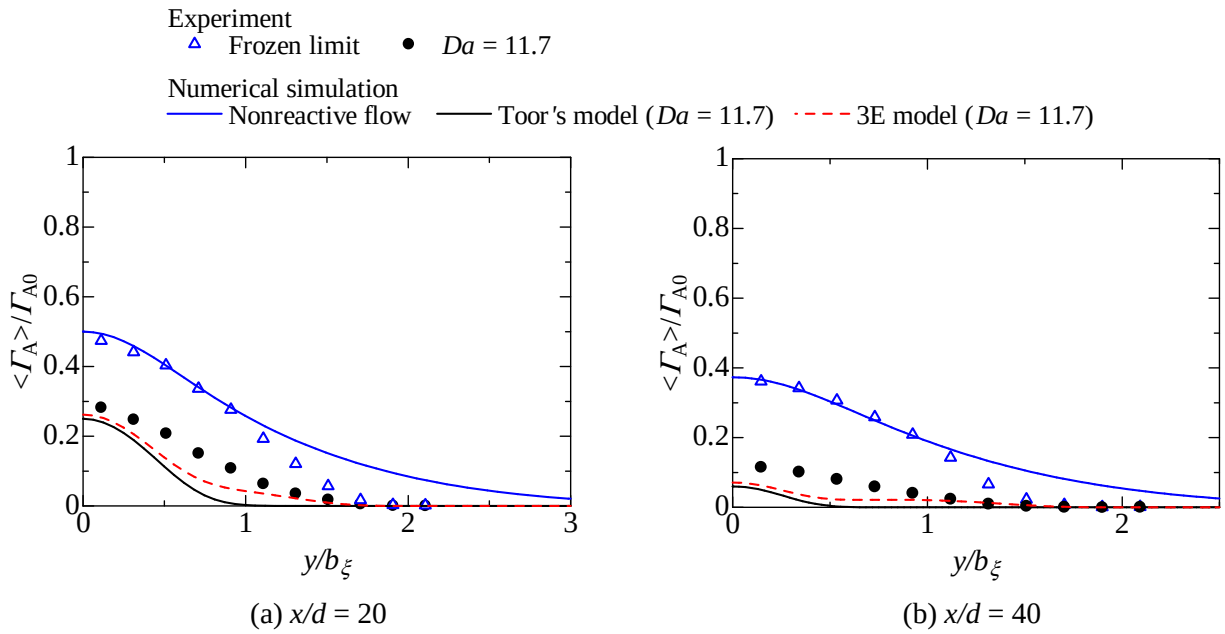

FIG. 24. Comparison of the mean concentration of the reactant A between the experiment and the numerical simulation using the Toor's model or the 3E model. (a) Cross-streamwise profiles at $x/d = 20$. (b) Cross-streamwise profiles at $x/d = 40$.